Lacustrine diatom oxygen isotopes as palaeo precipitation proxy - Holocene environmental and snowmelt variations recorded at Lake Bolshoye Shchuchye, Polar Urals, Russia

Hanno Meyer[1], Svetlana S. Kostrova[1], Philip Meister[1], Marlene M. Lenz[2], Gerhard Kuhn[3], Larisa Nazarova[1,4], Liudmila S. Syrykh[5], Yury Dvornikov[6].

[1] Alfred Wegener Institute Helmholtz Centre for Polar and Marine Research, Research Unit Potsdam, Telegrafenberg A45, Potsdam 14473, Germany

[2] Institute of Geology and Mineralogy, University of Cologne, Zülpicher Str. 49a, Cologne 50674, Germany

[3] Alfred Wegener Institute Helmholtz Centre for Polar and Marine Research, Am Alten Hafen 26, Bremerhaven 27568, Germany

[4] Kazan Federal University, Kremlyovskaya str. 18, Kazan 420018, Russia

[5] Herzen State Pedagogical University of Russia, Moika 48, St. Petersburg 191186, Russia

[6] Department of Landscape Design and Sustainable Ecosystems, Agrarian-Technological Institute, Peoples' Friendship University of Russia (RUDN University), 6 Miklukho-Maklaya St, Moscow, 117198, Russia.

Corresponding author: Hanno Meyer (hanno.meyer@awi.de). ORCID: 0000-0003-4129-4706

Key Points:

- Diatom oxygen isotopes from sediments of Lake Bolshoye Shchuchye are valuable proxies for the Holocene hydrological and climate dynamics
- Centennial-scale variability of the Holocene diatom isotope record is contemporaneous to glacier advances in the Northern hemisphere
- Snow melt variability in the lake catchment is the main driver for the short-term changes in $\delta^{18}O_{diatom}$

Abstract

The diatom oxygen isotope composition ($\delta^{18}O_{diatom}$) from lacustrine sediments helps tracing the hydrological and climate dynamics in individual lake catchments, and is generally linked to changes in temperature and $\delta^{18}O_{lake}$. Lake Bolshoye Shchuchye (67°53'N; 66°19' E; 186 m a.s.l) is the largest and deepest freshwater reservoir in the Polar Urals, Arctic Russia. Its $\delta^{18}O_{diatom}$ record generally follows a decrease in summer insolation and the northern hemisphere (NH) temperature history. However, it displays exceptional, short-term variations exceeding 5‰, especially in Mid and Late Holocene. This centennial-scale variability occurs contemporaneously with and similarly to Holocene NH glacier advances. However, larger Holocene glacier advances in the Lake Bolshoye Shchuchye catchment are unknown and have not left any significant imprint on the lake sediment record. As Lake Bolshoye Shchuchye is deep and voluminous, about 30−50% of its volume needs to be exchanged with isotopically different water within decades to account for these shifts in the $\delta^{18}O_{diatom}$ record. A plausible source of water with light isotope composition inflow is snow, known to be transported in surplus by snow redistribution from the windward to the leeward side of the Polar Urals. Here, we propose snow melt and influx changes being the dominant mechanism responsible for the observed short-term changes in the $\delta^{18}O_{diatom}$ record. This is the first time such drastic, centennial-scale hydrological changes in a catchment have been identified in Holocene lacustrine diatom oxygen isotopes, which, for Lake Bolshoye Shchuchye, are interpreted as proxy for summer temperatures and palaeo precipitation.

Keywords

stable oxygen isotopes, hydrological fluctuations, biogenic silica, diatoms, climate change, chironomids, lake sediments

1. Introduction

The ongoing climate warming is currently being debated at scientific, political and social levels. Comparisons with past climatic conditions are generally used to assess the stability or instability of regional environments as well as the potential to predict possible trends of future climate change. This is important for policymakers today and for human well-being in the future as food and water supply, energy production and use largely depend on the successful reconstructions of climatic conditions that existed in the past (IPCC, 2014; NOAA NCEI, 2020).

Glaciers and ice or snow fields are visual indicators for climate changes in high mountain regions (Davis et al., 2009; Khromova et al., 2014, 2019; Solomina et al., 2015; WGMS, 2017). Their advances and retreats do not only significantly alter landscapes (Khromova et al., 2019), but can also increase risks of local hazards and natural disasters (Huggel et al., 2008; Petrakov et al., 2008; Khromova et al., 2019). Changes in glacier mass balances lead to rearrangements of local and regional water cycles (Koboltschnig & Schöner, 2011; Radić & Hock, 2014; Nazarova et al., 2021a) and may be linked to global sea level rise (Shahgedanova et al., 2012; Gardner et al., 2013).

The Ural Mountains are a north-to-south stretching range of more than 2,000 km, separating Europe and Asia. As such, it is an orographic barrier playing an important role for atmospheric moisture transport to the Eurasian Arctic (i.e. Svendsen et al., 2004). In this region, small glaciers are widespread, mainly in the Polar Urals (Kononov et al., 2005; Shahgedanova et al., 2012; Khromova et al., 2014; Solomina et al., 2015; Svendsen et al., 2019). Field-based and satellite observations revealed that significant changes in air temperature and precipitation in recent decades have caused a reduction of the glacier areas in the Polar Urals by 23% on average (Nosenko & Tsvetkov, 2003; Shahgedanova et al., 2012; Khromova et al., 2014; 2019). Although numerous studies have contributed to a better understanding of the climate and environmental history in the Polar Urals (Panova et al., 2003; Cremer et al., 2004; Andreev et al.,

2005; Jankovská et al., 2006; Solovieva et al., 2008; Regnéll et al., 2019; Nazarova et al., 2021b), the glacier fluctuations in this region are still very poorly investigated (Kononov et al., 2005; Solomina et al., 2010, 2015; Haflidason et al., 2019) and existing knowledge of the glacier dynamics history remains fragmentary (Mangerud et al., 2008; Astakhov, 2018; Svendsen et al., 2014, 2019). Thus, reliable proxy data are required to reconstruct the long-term glacial history of the region in more detail.

Continuous reconstructions of glacier size variations are based on information provided by different parameters from lake sediments, e.g. magnetic susceptibility, loss-on-ignition, grain-size variations, and chemical element contents (Dahl et al., 2003; Nesje, 2009; Nesje et al., 2014; Regnéll et al., 2019; Lenz et al., 2021). The oxygen isotope composition of diatoms ($\delta^{18}O_{diatom}$) has been widely used as a proxy for climate and hydrological changes in many studies (Swann and Leng, 2009; van Hardenbroek et al., 2018). Shifts in diatom oxygen isotope records (Kostrova et al., 2013, 2019, 2021; Meyer et al., 2015; Cartier et al., 2019), often reflect changes in lake water ($\delta^{18}O_{lake}$) related to variations in atmospheric precipitation patterns and/or in the hydrological conditions (evaporation, meltwater supply) in the catchment. $\delta^{18}O_{diatom}$, consequently, has a high potential to enhance our understanding of coupled glacier-lake dynamics beyond the instrumental records.

In the current study, $\delta^{18}O_{diatom}$ from Lake Bolshoye Shchuchye (Fig. 1) has been employed as novel proxy to trace environmental and climatic fluctuations in the Polar Urals through the Holocene. Our approach is supported by lake-internal proxies (i.e. chironomid and biogeochemical analyses) of the same sedimentary succession, complemented by modern isotope hydrology and isotope mass-balance modeling. The newly obtained $\delta^{18}O_{diatom}$ record is discussed in the context of other regional and hemispheric environmental reconstructions (Andreev et al., 2005; Jankovská et al., 2006; Regnéll et al., 2019; Svendsen et al., 2019; Lenz et al., 2021; Cowling et al., 2021) including glacier fluctuations in order to explore the response of the lake system to hydroclimate change.

2. Study area

Lake Bolshoye Shchuchye (67°53'N; 66°19' E; 186 m a.s.l) is the largest and deepest freshwater reservoir of the Polar Urals, Arctic Russia, located in the permafrost zone at the boundary between Europe and Asia (Fig. 1). The lake surface area is 11.8 km^2, with mean and maximum water depths of 78.2 m and 160.0 m, respectively (Pechkin et al., 2017). The lake basin consists of a tectonic, glacially-eroded and overdeepened V-shaped mountain valley (Kemmerich, 1966; Svendsen et al., 2019; Haflidason et al., 2019) orientated northwest to southeast (Fig. 1B). With an average width of 0.92 km (maximum of 1.35 km) and a length of 12.7 km (Bogdanov et al., 2004), the lake is clearly elongated in shape. The lake is surrounded by ridges which peak up to more than 1000 m (Kemmerich, 1966). The lake basin is characterized by steep slopes and a sharp increase in depth in the central part and more gentle slopes in the northwestern and southeastern parts (Kemmerich, 1966; Pechkin et al., 2017). The bedrock comprises Proterozoic-Cambrian basaltic and andesitic rocks in the eastern and northwestern parts of the catchment and Ordovician quartzite and phyllitic rocks in the southwestern catchment (Dushin et al., 2009; Lammers et al., 2019; Svendsen et al., 2019). The catchment area of ~227 km^2 consists of a narrow zone along the lake as well as a wider hinterland to the north (Bogdanov et al., 2004). The lake is a hydrologically open system fed by 12 ephemeral streams with Pyryanatanë River as the main inflow forming a delta at the lake's northern end (Bogdanov et al., 2004). The Bolshaya Shchuchya River outflows at the southern part of the lake (Fig. 1B). The annual runoff from the catchment area is around 0.13–0.15 km^3 a^{-1} and about 5–7 years of residence time are required to renew the whole volume of water (~1 km^3) stored in the lake basin (Haflidason et al., 2019).

Lake Bolshoye Shchuchye is monomictic with mixing occurring only during the very short summer periods (Svendsen et al., 2019). The lake water temperature is persistently low, reaching

1.2−3.1°C beneath the ice (Regnéll et al., 2019) and a mean surface water temperature not exceeding 10−14 °C even on very hot days in August (Mitrofanova, 2017; Vinokurova, 2017). The lake is typically ice-covered for more than half a year, from early October to ice-out in late June–early July (Kemmerich, 1966; Svendsen et al., 2019). The lake ecosystem is pristine, and not subject to anthropogenic impact and changes only under the influence of natural factors (Yermolaeva & Burmistrova, 2017).

The regional climate is continental and quite severe with long, cold winters and short, cool summers. The catchment is characterized by excessive moisture with a lack of heat (Morozova et al., 2006). The average annual air temperature is −6.3 °C (at the Bolshaya Khadata station (260 m a.s.l) located ~25 km to the south of Lake Bolshoye Shchuchye; Fig. 1A), ranging from −14.3 °C (winter) to +7.0 °C (summer) (Solomina et al., 2010). Annual precipitation amounts are around 610 mm with the sum of warm period precipitation of 70 mm on average (Solomina et al., 2010; Shahgedanova et al., 2012). There are a few cirque- and niche-type glaciers less than 1 km^2 in size near the lake catchment today (Solomina et al., 2010; Khromova et al., 2014; Regnéll et al., 2019). However, glaciers almost disappeared in response to the recent climate warming (Svendsen et al., 2019).

The hydroclimate in this region reflects the trajectories of prevailing air masses. Typically, westerly cyclones originating over the Northern Atlantic dominate in winter, bringing cloudy, windy weather and precipitation (Kemmerich, 1966; Kononov et al., 2005; Shahgedanova et al., 2012; Pischalnikova, 2016). These are also related to strong winds that cause snow redistribution within mountains and its accumulation on leeward slopes and depressions (Mangerud et al., 2008). In summer, dry continental air masses from the east provide conditions for relatively hot and dry weather, whereas incursions of northwesterly and northerly cyclones often cause rain and a sharp drop in air temperatures (Kemmerich, 1966; Kononov et al., 2005).

3. Materials and methods

160 3.1. Sediment recovery, core lithology and chronology

161 In April 2016, a 54-m-long sediment core (Co 1321; 67°53' N, 66°19' E; water depth: 136 m)
162 was retrieved from the central part of Lake Bolshoye Shchuchye using gravity and percussion
163 piston corers (UWITEC Ltd., Austria) from the central part of Lake Bolshoye Shchuchye (Fig.
164 1). The depth interval from 9.15 to 0 mcd (meter composite depth) of the core, consisting of grey
165 to brown fine-grained, diffusely layered, hemipelagic sediment intermitted by turbidite layers, is
166 the focus of this paper. A recent study (Lenz et al., 2021) demonstrated that the upper 9.15-m
167 part was deposited during the last ~11,400 years (calendar ages are used consistently in this
168 study), i.e. covers the Holocene interglacial. The age-depth relationship of the analysed part of
169 the Co1321 core is based on the surface age (AD 2016) and five AMS ^{14}C dates. The age model
170 was calculated with CLAM version 2.3.9 (Blaauw, 2010, 2021), which was run in R version
171 4.0.3 (R core Team, 2020). The Holocene onset at ~ 11.5 cal. ka BP is supported by the results of
172 pollen analysis. A detailed description of the age model and lake internal parameters of Lake
173 Bolshoye Shchuchye are given in Lenz et al. (2021).

174

175 3.2. Geochemical analyses

176 The Co 1321 core was X-ray fluorescence (XRF)-scanned at 1-mm resolution using an
177 ITRAX core scanner (Cox Analytical, Sweden) at the University of Cologne. Sub-sampling for
178 total carbon (TC) and total inorganic carbon (TIC) analyses was done in 8-cm intervals omitting
179 turbidites, which offers a temporal resolution of about 100 years between two samples. TC and
180 TIC contents were measured with a DIMATOC 2000 carbon analyser (Dimatec Corp.,
181 Germany). Total organic carbon (TOC) was calculated by subtracting TIC from TC (Lenz et al.,
182 2021).

183

184 3.3. Biogenic silica analysis, diatom preparation and contamination assessment

Biogenic silica (BSi) analysis was performed on 0.45 g of dry sediment sampled from Co 1321. Samples were ground and analysed for BSi using the automated sequential leaching method (Müller & Schneider, 1993) at the Alfred Wegener Institute Helmholtz Centre for Polar and Marine Research (AWI Bremerhaven, Germany). Biogenic opal was calculated from BSi assuming a 10% water content within the frustule (Mortlock & Froelich, 1989; Müller & Schneider, 1993).

A total of 48 Holocene sediment samples with an initial biogenic opal content (Fig. 2) above 8% were processed for $\delta^{18}O_{diatom}$ analysis. Diatom purification involved a multi-step procedure based on Chapligin et al. (2012a). First, sediment samples were heated to 50 °C in 35% H_2O_2 for three days to remove organic matter, before adding 10% HCl to eliminate carbonates. To separate diatoms from the detrital contaminants with higher density, samples were centrifuged in sodium polytungstate (SPT; $3Na_2WO_49WO_3 \cdot H_2O$) heavy liquid solution (at decreasing densities from 2.50 to 2.10 g cm^{-3}) at 2500 rpm for 30 minutes. The detritus was retained for a contamination assessment and $\delta^{18}O_{diatom}$ correction. Hardly soluble micro-organic and lighter contaminants were removed by applying an inverse separation with SPT of 2.05 g cm^{-3}. Purified diatoms were then washed in ultra-pure water using a 3 µm filter. Finally, samples were wet sieved using a Rhewum Schallfix nylon mesh and sonication system, resulting in two diatom size fractions (3−10 µm and >10 µm). Only the 3−10 µm fraction yielded sufficient material (>2 mg) to be used for $\delta^{18}O_{diatom}$ analysis.

Energy-Dispersive X-ray Spectroscopy (EDS) under a scanning electron microscope (SEM) at the German Research Centre for Geosciences (GFZ Potsdam, Germany) was used to assess contamination of all diatom samples (Chapligin et al., 2012a). The EDS data (Table 1; Fig. 2) indicate that all 48 purified samples contained sufficient diatom material and less than 2.5% Al_2O_3 (Chapligin et al., 2012a) to be analysed for $\delta^{18}O_{diatom}$. 32 samples were highly purified, comprising between 97.1 and 98.8% SiO_2, and 0.5–1.6% Al_2O_3, respectively. 16 samples were less pure with 94.8–96.8% SiO_2, and 1.3–2.0% Al_2O_3.

3.4. Diatom isotope analysis and $\delta^{18}O_{diatom}$ correction

The oxygen isotope composition of purified diatom samples (n = 48) and the detrital contaminant sub-samples (n = 5) were measured at the ISOLAB Facility at AWI Potsdam with a PDZ Europa 2020 mass spectrometer. Prior to isotope analysis, exchangeable oxygen was removed using inert Gas Flow Dehydration (iGFD) under Argon gas at 1100 °C, after Chapligin et al. (2010). Dehydrated samples were fully reacted using laser fluorination with BrF_5 as reagent to liberate O_2 (Clayton & Mayeda, 1963) and then directly measured against an oxygen reference sample of known isotopic composition. Replicate analyses of the calibrated working standard BFC (Chapligin et al., 2011) yielded $\delta^{18}O$ = +28.82±0.26‰ (n=76) indicating an accuracy and analytical precision corresponding to the method's long-term analytical reproducibility (1σ) of ±0.25‰ (Chapligin et al., 2010).

All measured diatom $\delta^{18}O$ values were contamination-corrected using the geochemical mass-balance approach (Swann & Leng, 2009; Chapligin et al., 2012a):

$$\delta^{18}O_{corr} = (\delta^{18}O_{meas} - \frac{\delta^{18}O_{cont} \cdot c_{cont}}{100}) / (\frac{c_{diatom}}{100}) \quad (1)$$

where $\delta^{18}O_{meas}$ is the original measured $\delta^{18}O$ value of the sample. $\delta^{18}O_{corr}$ is the measured $\delta^{18}O$ value corrected for contamination, with $\delta^{18}O_{cont}$ = +12.8±0.6‰ (n = 5), which represents the average $\delta^{18}O$ of the heavy detrital fractions after the first heavy liquid separation. The percentages of contamination (c_{cont}) and diatom material (c_{diatom}) within the analyzed sample are calculated using the EDS-measured Al_2O_3 content of the individual sample divided by the average Al_2O_3 content of the contamination (21.5±1.0% in heavy fractions, n = 5) and as (100%–c_{cont}), respectively.

3.5. Water sampling and stable water isotope analysis

During the drilling campaign, lake water samples were collected in a depth profile of the water column between the lake ice cover and bottom (n = 17), at the same location as the

sediment core (Fig. 1B). Additionally, a 2.0-m snow profile was sampled from the surface of the snowpack to ground level in 10–15 cm intervals (n = 20). Snow samples were melted at room temperature. All water samples were stored cool in airtight bottles prior to stable isotope analyses.

Hydrogen (δD) and oxygen ($\delta^{18}O$) stable water isotopes were analyzed at the AWI ISOLAB Facility, Potsdam, Germany with a Finnigan MAT Delta-S mass spectrometer using equilibration techniques with an analytical uncertainty (1σ) of better than ±0.8‰ for δD and ±0.1‰ for $\delta^{18}O$ (Meyer et al., 2000). The secondary parameter deuterium excess is calculated as $d = \delta D - 8 \cdot \delta^{18}O$ (Dansgaard, 1964). Data are given as per mil difference (‰) to V-SMOW and compared to the Global Meteoric Water Line (GMWL; Craig, 1961) and to the Local Meteoric Water Line (LMWL) based on Global Network for Isotopes in Precipitation data of Salekhard (GNIP; IAEA/WMO, 2021) as the nearest station.

3.6. Isotopic mass-balance modeling

Isotopic mass-balance modeling was performed simulating varying amount and isotopic composition of surface inflow as well as evaporative enrichment on Lake Bolshoye Shchuchye. The goal of this was to determine both the potential impact of these factors on lake water isotopic composition and the speed of the reaction.

Assuming constant lake volume and hydrological parameters, the lake water isotopic composition after a given time can be calculated according to Gonfiantini (1986):

$$\delta^{18}O_{lake} = \delta^{18}O_S - (\delta^{18}O_S + \delta^{18}O_0) * e^{-(1+mx)*\left(\frac{It}{V}\right)} \quad (2)$$

where $\delta^{18}O_0$ is the initial isotopic composition of lake water and $\delta^{18}O_S$ the steady-state composition approached over time. The latter can be expressed as:

$$\delta^{18}O_S = \frac{\delta^{18}O_I + mx\delta^{18}O^*}{1+mx} \quad (3)$$

The limiting isotope enrichment $\delta^{18}O^*$ is calculated according to Gat (1981), m and x represent the temporal enrichment slope and the fraction of lake water lost by evaporation,

respectively. For further elaboration on this approach, we refer to Darling et al. (2006) and references therein. The inflow isotopic composition $\delta^{18}O_I$ was assumed to be equal to $\delta^{18}O_0$ and to $\delta^{18}O$ of mean annual precipitation (-17.8‰). Mean annual precipitation and mean summer precipitation were modeled using the Online Isotopes in Precipitation Calculator (OIPC; Bowen, 2021), c.f. chapter 4.2. Since data for evaporation are not readily available, the amount of evaporation from the lake surface was approximated as a function of summer mean air temperature *T*, atmospheric humidity *h*, altitude *a* and latitude *A* (Linacre, 1977).

$$E_0 = \frac{700\frac{T_m}{100-A}+15(T-T_d)}{(80-T)} \left(\frac{mm}{d}\right) \quad (4)$$

where $T_m = T + 0.006a$ and the dew-point T_d is approximated according to Lawrence (2005) as $T_d \approx T - \left(\frac{1-h}{5}\right)$. Assuming an ice-free period of 100 days per year, the calculated daily evaporation rates were multiplied by 100 to obtain annual values. The isotopic composition of atmospheric moisture was calculated according to Gibson et al. (1999) based on summer precipitation.

3.7. Chironomid analysis

Eighty-four samples were prepared for chironomid analysis with standard techniques (Brooks et al., 2007). Chironomid identification followed Wiederholm (1983) and Brooks et al. (2007).

The ratio of lotic (moving water or riverine) and lentic (standing water) chironomid taxa in sediments of the Lake Bolshoye Shchuchye, and chironomid-inferred mean July air temperature (T_{air}) are in the focus of this study. In this context, increasing representation of the lotic fauna reflects stronger runoff and more intensive water input with the inflowing rivers (Nazarova et al., 2017c; Biskaborn et al., 2019). For information on ecology of chironomid taxa, we refer to Brooks et al. (2007), Stief et al. (2005), Moller Pilot (2009, 2013), and Nazarova et al. (2011, 2015, 2017a, b). The reconstruction of mean July air temperatures was performed using the

North Russian (NR) chironomid-based temperature inference model (WA-PLS, 2 component; r^2 boot = 0.81; RMSEP boot=1.43 °C) (Nazarova et al., 2015).

3.8. Digital elevation model preparation and delineation of the lake catchment

The freely distributed digital elevation model (DEM) ArcticDEM (Porter et al., 2018) was used for Lake Bolshoye Shchuchye catchment delineation and morphometric analysis of the catchment. Raw 10-m resolution ArcticDEM data covering the area of interest were downloaded from the Polar Geospatial Center data portal (https://www.pgc.umn.edu/data/arcticdem/). Contours at 20-m intervals were extracted from the DEM and were manually corrected for artefacts and missing patches in order to build up a hydrologically correct digital terrain model (DTM). This improved DTM was created by interpolating corrected contours using the TopoToRaster algorithm with drainage enforcement (Hutchinson, 1989) within the ESRI© ArcGIS 10.2 software. The catchment of Lake Bolshoye Shchuchye was extracted based on the hydrologically correct topographic representation within QGIS 3.10 software. For morphometric analysis, topographic variables were obtained, including slopes, aspects, total curvature, flow direction, flow accumulation. All topographic variables were calculated with R (R Core Team, 2017) using the packages 'raster' (Robert & van Etten, 2012), 'dynatopmodel' (Quinn et al., 1995) and 'spatialEco' (Evans, 2020).

3.9. Calculation of the snow water equivalent within the catchment

The catchment polygon was further used to analyze the distribution of snow depth and snow water equivalent (SWE). Snow depth within the lake catchment at 10-m resolution was calculated using auxiliary data: cumulative snow probability for snow melt period of 2019 extracted from Sentinel-2 time series and snow depth ranges (0–845 cm of snow) measured within ten snow survey profiles within the neighboring lake Bol'shaya Khadata catchment (Gokhman & Zhidkov, 1979). The atmospherically corrected (sen2cor, ESA) Sentinel-2 Level-

2A data archive was analyzed in order to calculate the cumulative snow probability value for the entire catchment. Level-2A data provide the snow probability band scaled from 0 to 1 based on the specific spectral signature of snow cover, where values of 0 and 1 correspond to 0% snow and 100% snow, respectively. For the 2019 glaciological year (October–May; Ivanov, 2013), we obtained all images (less than 20% clouds) and filtered out all scenes covering less than 85% of the lake catchment without clouds. Further, all snow probability bands of these images were summarized to calculate a cumulative value: there were seven scenes meeting the requirements covering the period from May 8, 2019 (maximum of snow) to July 25, 2019 (quasi-complete melting of snow). Within the range of cumulative snow probability, the range of snow depth was scaled to measured snow depths of the neighboring catchment in 1978 (Gokhman & Zhidkov, 1979). The SWE was calculated based on the empirical relationship between snow depth and SWE obtained for tundra landscape in Central Yamal (500 km to the North from the lake) according to Dvornikov et al. (2015). All satellite image analysis and calculations were performed within Google Earth Engine Cloud Computing platform (Gorelick et al., 2017).

4. Results

4.1. Stable water isotopes

The results of stable water isotope analyses are presented in a $\delta^{18}O$–δD diagram (Fig. 3). One water sample taken directly at the ice-water boundary (Fig. 4A) and one surface snow sample (Fig. 4C) were excluded from interpretation due to significantly different isotopic signals from those for other samples; likely due to interaction between water phases. The average recent water isotope composition of Lake Bolshoye Shchuchye is −15.9±0.2‰ for $\delta^{18}O_{lake}$, −114.4±2.6‰ for δD_{lake} and +13.0±0.5‰ for *d* excess (n = 16). The water column $\delta^{18}O$-profile reveals no substantial changes with depth (Fig. 4A). Small variations of 0.5‰ were detected at 10 m depth, incoherent with T_{lake} changes (Fig. 4B). A positive (0.08 ‰/°C), but statistically not significant ($R^2 = 0.14$) correlation was found between $\delta^{18}O_{lake}$ and T_{lake}.

340 The snow cover displays a large variability between single layers in their $\delta^{18}O_{snow}$ and δD_{snow}
341 values ranging from −25.1 to −15.2‰ and from −190.1 to −103.1‰, respectively. The *d* excess
342 ranges from +2.7 to +18.9‰. The minimum $\delta^{18}O_{snow}$ with −25.1‰ is reached at the depth of 115
343 cm. $\delta^{18}O_{snow}$ values demonstrate a continuous decrease of ~0.07‰/cm in the lower (195−115
344 cm) part of the column (Fig. 4C). Visible variations in $\delta^{18}O_{snow}$ with smaller maxima at depths of
345 10, 75 and 105 cm occur in the upper section (115−0 cm) of the core. In general, this interval
346 displays a gradual increase of ~0.09‰.cm^{-1} in $\delta^{18}O_{snow}$ values.
347 As precipitation samples could not be collected at Lake Bolshoye Shchuchye, mean annual
348 $\delta^{18}O_{prec}$ and δD_{prec} values of regional precipitation have been derived from the GNIP database
349 (IAEA/WMO, 2021) for Salekhard (16 m a.s.l) situated ~150 km southeast of the lake (Fig. 1A).
350 Additionally, $\delta^{18}O_{prec}$ and δD_{prec} values as well as a LMWL were modelled for the drilling
351 location based on the algorithm published by Bowen and Revenaugh (2003) and Bowen et al.
352 (2005) using the OIPC (Bowen, 2021). Modelled $\delta^{18}O_{prec}$ and δD_{prec} values of −17.8±0.4‰ and
353 −135.0±3.0‰ (Bowen, 2021) are consistent with GNIP values of −17.5±1.7‰ and
354 −136.1±13.2‰, respectively (IAEA/WMO, 2021). The LMWL based on modelled values was
355 determined as: $\delta D = 7.7\ \delta^{18}O + 2.6‰$ ($R^2 = 1.00$; Fig. 3; Bowen, 2021) and is in a good
356 agreement with the LMWL from GNIP data (IAEA/WMO, 2021) with a slope of 7.9 and an
357 intercept of +1.2‰ ($R^2 = 0.99$; Fig. 3). Minor offsets between the LMWLs are mainly due to
358 differences in both temporal and spatial domains. Due to the distance of Salekhard to the
359 sampling location, we assume the modelled $\delta^{18}O_{prec}$ and δD_{prec} values and the LMWL to be more
360 reliable for Lake Bolshoye Shchuchye.
361
362 4.2 Oxygen isotope record
363 The Lake Bolshoye Shchuchye diatom $\delta^{18}O_{corr}$ values (further referred to as $\delta^{18}O_{diatom}$) range
364 from +23.4‰ to +31.8‰ (Fig. 4; Table 1) and exhibit the same trend as $\delta^{18}O_{meas}$ values.
365 Contamination correction leads to an offset of $\delta^{18}O_{corr}$ towards higher values of about 0.7‰ in

366 the upper part of the core (younger than 8.5 cal. ka BP) and 1.3‰ higher for the lower part (older
367 than 8.5 cal. ka BP).

368 The Co 1321 core is characterized by a mean $\delta^{18}O_{diatom}$ value of +27.0‰ for the complete
369 Holocene. In Early Holocene (11.4 to 7 cal. ka BP), the $\delta^{18}O_{diatom}$ values are with +27.3±0.8‰
370 slightly higher than the Holocene mean. Highest mean $\delta^{18}O_{diatom}$ values with +27.9±2.0‰ are
371 observed in Mid Holocene (7 to 5 cal. ka BP), whereas lowest $\delta^{18}O_{diatom}$ values of +26.3±1.7‰
372 characterize the Late Holocene (5 cal. ka BP to present). The maximum $\delta^{18}O_{diatom}$ value
373 (+31.8‰) in the record is registered at 6.3 cal. ka BP. The absolute minimum in the $\delta^{18}O_{diatom}$
374 record occurs at the sediment surface at 0.0 cal. ka BP with +23.7‰. Sharp variations are
375 observed every ~0.7–1.5 cal. ka with smaller maxima at 1.0, 1.9, 2.6, 3.7, 4.6, 6.4, 7.1, 8.1, 9.2,
376 10.1 and 10.5 cal. ka BP and smaller minima at 1.7, 2.4, 3.0, 4.1, 5.8, 6.6, 7.3, 8.3, 10.4 and 10.9
377 cal. ka BP. In general, a gradual depletion of ~0.39‰/1000 years is visible between 10.9 and 0.0
378 cal. ka BP (Fig. 4).
379
380 4.3 Chironomids
381 The chironomid fauna of Lake Bolshoye Shchuchye is dominated by cold-tolerant lentic taxa
382 usual for Arctic lakes. Several taxa characteristic for lotic environments have been found in the
383 lake sediments. Among them are taxa from the subfamilies Diamesinae (e.g. *Diamesa aberrata*-
384 type, *D. cinerella*-type, *D. bertrami*-type), that usually inhabit small, cold running streams and
385 brooks and Orthocladiinae (e.g. *Eukiefferiella*, *Metriocnemus*, *Thienemanniella clavicornis*-type,
386 *Tvetenia bavarica*-type), that occur in flowing waters and surf zones of the lakes.
387 Representation of the lotic taxa varies considerably reaching 50% of the fauna during the
388 Early Holocene (at ~10.6 cal. ka BP) (Fig. 4). However, rather high concentration of lotic
389 chironomids (25−33% of the fauna) have been observed between 7.7 and 4.5 cal. ka BP.
390 Between 4.5 and 3.2 cal. ka BP, no lotic taxa appear in the lake, indicating a decrease of the
391 water inflow (Fig. 4). At 3.2 cal. ka BP, lotic chironomids appear in the lake again and their

abundance reaches 25% of the fauna. Between 3.2 and 0 cal. ka BP, the abundance of lotic taxa remains at 11% in average, and it rises to 31% towards the modern times.

The chironomid-based reconstructed T_{air} during the Early Holocene are in average ~1.5 °C below modern level. The transition to the Mid Holocene is characterized by an increase in chironomid abundancies with a gradual rise in the reconstructed T_{air} to the modern level (10.6 °C). Between ~8.0 and 3.2 cal. ka BP, the T_{air} are the highest and reach up to 3 °C above the present T_{air} at 5.5 cal. ka BP. However, there is a cooling tendency in T_{air} after 5.5 cal. ka BP, when reconstructed T_{air} gradually decrease and reach ~1 °C below the modern T_{air} at ~1.7 cal. ka BP. Chironomid-based reconstructed T_{air} are slightly above modern values between 1.0 to 0.6 cal ka BP, subsequently decreasing to the present level.

5. Discussion

5.1. Isotope hydrology

When interpreting lacustrine $\delta^{18}O_{diatom}$ records, a proper understanding of the modern hydrology is a precondition for assessing possible past hydrological changes.

The recent mean Bolshoye Shchuchye $\delta^{18}O_{lake}$ of −15.8‰ is slightly higher than the regional $\delta^{18}O_{prec}$ of −17.8‰ (Bowen, 2021). Additionally, the lake water isotope samples plot on the GMWL and slightly above the modelled LMWL (Fig. 3) and follow a linear dependency with a slope of 7.2 and an intercept of +0.3 (R^2 = 0.90; n = 16). This suggests that $\delta^{18}O_{lake}$ roughly corresponds to $\delta^{18}O_{prec}$, slightly shifted to more positive values probably due to seasonality effects.

At the same time, water samples are situated close to the GMWL (Fig. 3), indicating the absence of major evaporation effects in recent times. The V-shape of the lake basin, almost completely surrounded by steep slopes, allows for lake level fluctuations without significant changes in the lake surface area and water volume.

Palaeogeographical and geomorphological studies yielded pre-Holocene Bolshoye Shchuchye lake level fluctuations with a highstand 8 m above present lake level along parts of the western shore (Svendsen et al., 2019). This higher than modern lake level might have resulted from intense meltwater influx from contemporaneous glaciers in the lake catchment and a simultaneous damming of the lake by a glacifluvial fan at the south outlet until around 14−15 cal. ka BP (Svendsen et al., 2019). The lake level dropped when this fan was incised by glacial meltwaters (Regnéll et al., 2019). Additionally, seismic profiles point to lower lake levels prior to 15 cal. ka BP (Haflidason et al., 2019). A terrace in the northern part of Lake Bolshoye Shchuchye documents a 2–3 m higher lake level at ~2–3 cal. ka BP (Svendsen et al., 2019). Therefore, lake level changes and associated evaporation effects cannot be fully excluded at Lake Bolshoye Shchuchye, especially during the Last Glacial Maximum and the early deglaciation period, but are assumed to be weak for the Holocene, the period of interest.

The water $\delta^{18}O_{lake}$ depth profile shows a constant isotope composition (Fig. 4A) and suggests a well-mixed water column lacking any isotopic stratification, at least in spring 2016. There is no notable relationship between $\delta^{18}O_{lake}$ and T_{lake} (Fig. 4A, B). Hence, water column temperature effects are assumed to be of minor importance on $\delta^{18}O_{lake}$.

The snow cover isotope samples plot on or close to the GMWL (Fig. 3) in the co-isotope diagram with a slope of 7.9 and an intercept of +10.8 (R^2 = 0.96). The mean $\delta^{18}O_{snow}$ of −20.4‰ (*d* excess = +12.9‰) is slightly higher than the regional mean $\delta^{18}O_{prec}$ of −22.8‰ (*d* excess = +8.4‰) between October and April (when precipitation fall as snow) derived from the OIPC (Bowen, 2021). This likely represents a seasonal bias towards late winter and spring snow, but could also include effects of sublimation, evaporation and wind drift processes altering the snow pack's isotopic composition over time (Friedman et al., 1991; Nikolaev & Mikhalev, 1995). The $\delta^{18}O_{snow}$ profile displays variations with depth (Fig. 4C) which might be associated with isotopic differences between individual precipitation (or deposition) events persisting despite snow metamorphism (Friedman et al., 1991). Nevertheless, as T_{air} is a primary control of $\delta^{18}O_{prec}$

especially in polar regions (Dansgaard, 1964), it is likely that the isotopically lightest layers (110−130 cm) with $\delta^{18}O_{snow}$ of −24 to −25‰ were formed during the coldest months (January−February). Generally, it can be concluded that snow can be a source of isotopically-depleted water draining into the lake.

In summary, Lake Bolshoye Shchuchye is a well-mixed, non-evaporative and isotopically rather uniform lake, which is mainly fed by meteoric waters, i. e. precipitation with an important contribution of melting snow from higher altitudes. Although there are indications of evaporation effects in the past, we suggest the precipitation signal ($\delta^{18}O_{prec}$) to be most relevant for $\delta^{18}O_{lake}$.

5.2. Isotope fractionation and main controls on $\delta^{18}O_{diatom}$

Variations in $\delta^{18}O_{diatom}$ values of lacustrine sediment are mainly controlled by changes in water temperature (T_{lake}) and/or the corresponding $\delta^{18}O_{lake}$ (Labeyrie, 1974; Juillet-Leclerc & Labeyrie, 1987; Leng & Barker, 2006; Dodd & Sharp, 2010).

When comparing the overall Holocene average Lake Bolshoye Shchuchye $\delta^{18}O_{diatom}$ of +27.0‰ with the recent average $\delta^{18}O_{lake}$ of –15.9‰, a fractionation coefficient $\alpha_{(silica\text{-}water)} = (1000 + \delta^{18}O_{diatom})/(1000 + \delta^{18}O_{lake})$ (Juillet-Leclerc & Labeyrie, 1987) of 1.0436 was determined. This yields an isotopic enrichment $\Delta^{18}O_{SiO2\text{-}H2O}$ = 42.9‰ corresponding to a T_{lake} of 4.5 °C that matches well the blooming temperature of the diatom species *Aulacoseira subarctica* (~4 °C; Gibson et al., 2003; Lepskaya et al., 2010) dominant in the sediments of the lake (A. Ludikova, pers. comm.). This suggests that the $\delta^{18}O_{diatom}$ values at Lake Bolshoye Shchuchye (Table 1), are the right order of magnitude and, consequently, underline the general applicability of the diatom isotope signal for palaeoreconstructions at the lake.

To test whether temperature effects are the dominant forcing responsible for the short-term variability in $\delta^{18}O_{diatom}$ of up to 5‰, we calculated a scenario function displaying possible changes in T_{air} and T_{lake}. We used the aforementioned $\delta^{18}O_{diatom}$-temperature coefficient of −0.2‰/°C (Dodd & Sharp, 2010) and the regional temperature relation between monthly mean

469 $\delta^{18}O_{prec}$ and T_{air} of $\delta^{18}O_{prec}$ = +0.34‰/°C (Salekhard; IAEA/WMO, 2021). The scenario function
470 for a 5‰-shift as visible in the Bolshoye Shchuchye diatom isotope record constitutes a linear
471 function, the slope of which is defined by the quotient of the T_{lake} and T_{air} coefficients (Figure
472 S1). Intercept and Zero of the function represent ”traditional” interpretations of temperature
473 effects regarding either T_{lake} or T_{air} alone, respectively. The former suggests a drop in T_{lake} of
474 25°C while the latter corresponds to a rise in T_{air} of 14.7°C needed to explain the shifts of 5‰ in
475 $\delta^{18}O_{diatom}$. Due to the fact that present lake temperature changes in the course of an annual cycle
476 amount to 7−11 °C only (Mitrofanova, 2017; Vinokurova, 2017; Regnéll et al., 2019), variations
477 of 25°C during the summer period (diatom bloom) are highly unlikely. Consequently, T_{lake} alone
478 cannot be the primary control and rather plays a subordinate role in explaining $\delta^{18}O_{diatom}$ in Lake
479 Bolshoye Shchuchye. Similarly, a 14.7°C increase in T_{air} is unlikely and contrasts with only ~3-4
480 °C from pollen reconstructions (Andreev et al., 2005) and maximum 6°C from the current
481 chironomid-based reconstruction for the complete Holocene (Fig. 4). Other mathematically
482 possible combinations of T_{air} and T_{lake} (points plotting on the scenario function) are not plausible
483 either as they would require even more pronounced changes of T_{air} and T_{lake}.

484 Since Lake Bolshoye Shchuchye currently does not show evaporative enrichment, we
485 conclude the isotopic composition of the inflow to be main driver of the lake water isotopic
486 composition and, hence, of the $\delta^{18}O_{diatom}$ record. Inflow, in turn, largely reflects precipitation, but
487 with temperature effects ruled out as the single decisive factor, such changes can only be
488 attributed to atmospheric circulation changes or hydrological processes within the lake’s
489 catchment.

490 Reorganization of the atmospheric transport patterns in Early Holocene after the decay of the
491 Eurasian Ice Sheet around ~10 cal. ka BP, allowed moisture from the North Atlantic to enter the
492 region, in line with the northward migration of the treeline. Forest conditions persisted in the
493 catchment until ~4 cal. ka BP, when the treeline retreated back south (Clarke et al., 2020).
494 Today, westerly/northwesterly cyclones originating over the Atlantic (the Northern and

Norwegian seas) moving across Scandinavia to the Taymyr Peninsula bring relatively warm and moist air masses to the Polar Urals year-round, especially in winter (Kononov et al., 2005; Shahgedanova et al., 2012; Pischalnikova, 2016). Relatively cold northerly cyclones forming around the Novaya Zemlya archipelago over the Barents and Kara seas deliver comparably less moisture (Kononov et al., 2005; Morozova et al., 2006). However, this northerly influence might have increased over the Holocene with a reduced sea ice concentration in the Kara and Barents Sea sectors. Moreover, recycled moisture from regional terrestrial surface waters might contribute through evaporation/evapotranspiration in summer (Bonne et al., 2020) in line with the establishment of forests in the catchment. Changes in the relative contribution of these moisture sources to the local water balance can therefore shift $\delta^{18}O_{lake}$ and $\delta^{18}O_{diatom}$ both towards higher and lower $\delta^{18}O$ values, but relative changes should be visible in regional palaeoenvironmental reconstructions. In summary, the changes in the Lake Bolshoye Shchuchye $\delta^{18}O_{diatom}$, are mainly driven by changes in $\delta^{18}O_{lake}$ signal, affected by T_{air}, atmospheric circulation and local hydrological conditions.

5.3. The Bolshoye Shchuchye $\delta^{18}O_{diatom}$ record

The diatom isotope record displays higher overall values of +27.4±1.3‰ in Early- to Mid-Holocene (with the absolute maximum $\delta^{18}O_{diatom}$ of +31.8‰ at 6.4 cal. ka BP) and lower values of +26.4±1.7‰ in Mid- to Late Holocene (with a clear minimum of +23.2‰ at the surface corresponding to the most recent, ~100 years old sediments). Generally, a gradual decrease in $\delta^{18}O_{diatom}$ of ~3–4‰ over the Holocene is notable in the Bolshoye Shchuchye $\delta^{18}O_{diatom}$ record, especially when considering the minima (Fig. 4). This is in line with the summer insolation decrease at 60°N (Berger & Loutre, 1991). Insolation reaches a maximum in Early Holocene and a minimum in Late Holocene, i.e. during the Little Ice Age (LIA). The high overall variability in the Bolshoye Shchuchye $\delta^{18}O_{diatom}$ record ($\Delta^{18}O$ of 8.6‰) results from both this trend with

520 higher $\delta^{18}O_{diatom}$ values in the first half of the Holocene and lower values in the Late Holocene as
521 well as short-term fluctuations superimposed upon this trend.

522 These fluctuations consist of short term (centennial-scale) maxima and minima of more than
523 5‰, setting the Bolshoye Shchuchye $\delta^{18}O_{diatom}$ record apart from most other diatom isotope
524 records stemming from high-latitude open lakes. Since these variations in $\delta^{18}O_{diatom}$ are in most
525 cases based on more than one data point they are unlikely to be artefacts related to sample
526 preparation or contamination correction issues.

527 The key questions are (1) which processes may be responsible for these short-term variations
528 in $\delta^{18}O_{diatom}$ and (2) whether these processes are related to a larger scale pattern, visible in other
529 lake-internal proxies and beyond or rather singular observations for Lake Bolshoye Shchuchye.

530 Generally, high-latitude lacustrine diatom isotope records from open lakes are rather smooth
531 depending on depth, volume and residence time of the lake under consideration (Swann et al.,
532 2010; Chapligin et al., 2012b; Kostrova et al., 2019, 2021). These records vary usually by 3–5‰
533 over the entire Holocene and have been interpreted taking into account the individual
534 hydrological situation and isotopic background of each lake. As a consequence, short-term
535 fluctuations seldomly exceed 2‰ and have been found (but not interpreted) as single-point
536 spikes in Lake Kotokel, a very shallow, highly evaporative lake (Kostrova et al., 2013, 2014).
537 Moreover, two short-term negative excursions of 4-5‰ have been described in a published
538 $\delta^{18}O_{diatom}$ record only, at 4.7 and 1.4 cal. ka BP for Lake Chuna on Kola Peninsula (Jones et al.
539 2004).

540 Isotopic mass-balance modeling (Fig. 5) shows the potential impact of evaporative
541 enrichment on Lake Bolshoye Shchuchye for three different scenarios, ranging from present
542 conditions to hypothetic much lower annual precipitation and atmospheric humidity. While
543 evaporation can indeed impart an effect of ~2‰ within several decades, it fails to reproduce the
544 magnitude of the short-term fluctuations observed in the Lake Bolshoye Shchuchye record.

545 The difference between present-day conditions (precipitation 610 mm/a, h=0.9) and the most
546 arid, hypothetic scenario (200 mm/a, h=0.7) amounts to an isotopic enrichment of only 1.85‰.
547 These results, in conjunction with the fact that Lake Bolshoye Shchuchye currently does not
548 exhibit an evaporative signature, suggest that there must be a different locally-confined influence
549 on the water isotope composition to explain the minima and maxima in the $\delta^{18}O_{diatom}$ record.
550 Large-scale atmospheric patterns (i.e. shifts in the moisture transport and precipitation
551 regime, seasonality of precipitation) seem unlikely as they would have an influence on a larger
552 region that should be visible in other proxies and regional datasets as well and would lead to
553 rather moderate changes. Changes in lake ice coverage, and hence, seasonality of the diatom
554 bloom seem also unlikely processes as these would also change moderately in a deep basin as
555 Lake Bolshoye Shchuchye.
556 For a significant change in the isotope composition of a lake, another option is substitution of
557 lake water, i.e. a certain volume being replaced by isotopically different water. In mountainous
558 areas such as the Polar Urals, water of lighter isotope composition than the lake itself might be
559 glacier or snow melt waters draining from higher altitudes into the lake (i. e. Meyer et al., 2015).
560 Taking into account the recent $\delta^{18}O_{lake}$ of -15.8‰ and assuming the present-day volume as
561 constant and 100%, it can be calculated, how much water needs to be exchanged in Lake
562 Bolshoye Shchuchye to explain an isotopic difference $\Delta^{18}O$ of 5‰. If this isotopically different
563 inflow would correspond to the lightest snow measured within the catchment (-25‰; Fig. 3C),
564 corresponding to a ~10‰ offset compared to $\delta^{18}O_{lake}$, about 55% of the lake water (equal to 0.55
565 km^3) need to be exchanged. Assuming lower snow endmember values of -30‰ and -35‰, less
566 water would need to be replaced, but still amounting to 35% and 26% of the lake volume,
567 respectively.
568 Adding large amounts of water from a different than usual source (with different water
569 isotope composition) or cutting off the major source for a certain period could, hence,
570 substantially change the isotope composition of the lake. At Two-Jurts-Lake (Kamchatka), the

diatom isotope composition follows summer insolation, but changes in Neoglacial times due to the addition of isotopically light water from melting glaciers (Meyer et al., 2015) even though there is currently no glaciation in the catchment. The more glacial meltwaters reach the lake, the more negative the inflow $\delta^{18}O$ and, hence, $\delta^{18}O_{lake}$. Less meltwater would imply lower contribution of isotopically light influx. If Lake Bolshoye Shchuchye received large amounts of meltwater, this should be notable both in the sediment and hydrological records.

5.4. Glacier fluctuations

Glacier fluctuations are poorly constrained in the Russian Arctic, including the Polar Urals (Kononov et al., 2005; Solomina et al., 2010, 2015; Haflidason et al., 2019). It is known though that the glaciers in the Urals display exceptional changes in local accumulation (and ablation) budgets (Mangerud et al., 2008). Westerlies, especially in the winter season, favor accumulation of snow on leeward sides of the mountains. This process, combined with snow avalanches, leads to extremely high local accumulation rates, which may be several times higher than local precipitation (Mangerud et al., 2008). Therefore, the situation on leeward sides of the Ural Mountains allows for short-term changes of the local accumulation and water balance, and hence, implies the possibility of contribution of light isotopic (winter and/or high altitude) precipitation to the lake.

Svendsen et al. (2019) performed a detailed assessment of the glacial and environmental changes in the Polar Urals including geomorphological description, exposure ages and lake sediment coring. In their study, they concluded on a larger glaciation in the region during stage MIS 4, and more restricted mountain glaciers in MIS 2 and MIS 3, but only small glaciers in shaded areas of the Polar Urals during MIS 1 that formed during Late Holocene cooling. For the Ural Mountains, an endmoraine and glacier advances during the Little Ice Age (LIA) age have been described (Mangerud et al., 2008).

A possibility to test our hypothesis of glacial meltwaters triggering centennial-scale changes in $\delta^{18}O_{lake}$ is a comparison with northern hemispheric (or Eurasian) glacial fluctuations as summarized in Solomina et al. (2015). Here, the Russian Arctic is poorly constrained, but several glacial advances have been described in Neoglacial times, generally associated with regional cooling i.e. for Franz Josef Land with a prominent advance in the LIA (Lubinsky et al., 1999). However, regional compilations of dated glacier advances exist for the Alps (Ivy-Ochs, 2009), Scandinavia (Nesje, 2009) or semi-arid Asia (Dortch et al., 2013), summarized in Solomina et al. (2015).

Especially striking is the similarity to the Scandinavian reconstruction (Nesje, 2009) with described glacial advances at 0.2–0.7, 1.6, 2.3, 3.3, 4.4, 5.6 cal. ka BP, corresponding to prominent minima in the Bolshoye Shchuchye $\delta^{18}O_{diatom}$ record (Fig. 4), which would correspond to enhanced influx of glacial meltwaters, either due to more winter precipitation or meltwater entering the lake lowering $\delta^{18}O_{lake}$. Other prominent minima in the $\delta^{18}O_{diatom}$ record at 6.6–6.8 and 7.4–7.7 cal. ka BP are, however, not found in the Scandinavian reconstruction by Nesje (2009), but either in the Alps, in Norway (Matthews & Dresser, 2008) or in semi-arid Asia (Dortch et al., 2013).

The centennial-scale fluctuations in the $\delta^{18}O_{diatom}$ record are contemporaneous with northern hemisphere glacier advances, described for other Eurasian regions. Therefore, maxima in the Bolshoye Shchuchye $\delta^{18}O_{diatom}$ record could hence be associated with either reduced meltwater or winter precipitation influx to the lake either due to lower precipitation amounts or less snow transported to the leeward side of the Ural Mountains.

High-resolution glacier mass balance studies in the Polar Urals provide (additional) evidence for short-term snow changes in the region, with a generally positive glacier mass balance in the Little Ice Age (LIA) and a negative mass balance after 1850 (Kononov et al., 2005). LIA moraines have been described for several glaciers in the Polar Urals, including the Chernov and Obruchev glaciers (Mangerud et al., 2008). The second part of the 20th century shows a

622 pronounced tendency towards glacier shrinkage, with solid precipitation in the region being
623 generally lower than the ablation (Khromova et al., 2014; 2019).
624
625 5.5. Lake-internal parameters
626 In order to test whether the strong variability in the Holocene $\delta^{18}O_{diatom}$ record at Lake
627 Bolshoye Shchuchye with their clear, short-term centennial-scale fluctuations is also reflected in
628 the lakes' sedimentary record, we inter-compare diatom isotopes and lake-internal parameters
629 from Lenz et al. (2021). These parameters (Fig. 4) supposedly react on fast and major changes in
630 the catchment hydrology and include abiotic (clay content and Ti cps) as well as biotic proxies
631 (TOC, biogenic opal contents and chironomids).
632 All these proxies display some internal variability throughout the Holocene, but do not
633 reveal statistically significant relationships with the $\delta^{18}O_{diatom}$ record. During the Early
634 Holocene the observed high representation of lotic chironomids can be related to a very poor
635 lacustrine fauna at this time. Lotic chironomids are brought by riverine influx, i.e. fed by water
636 from snowmelt and enrich the lake benthic communities. Decrease in the share of lotic taxa
637 thereafter can be related to a better development of the lacustrine fauna under milder climatic
638 conditions during the Mid Holocene. At ~7.5 to 8.5 cal. ka BP, when $\delta^{18}O_{diatom}$ shows a
639 maximum and the diatom isotope variability increases clearly, a major phase shift is obvious in
640 all lake-internal proxies with absolute maxima in biogenic opal, TOC and chironomid-derived
641 summer T_{air}, as well as absolute minima in Ti and clay values.
642 At 7.5 cal. ka BP, the lake-internal parameters show a slight decrease in biogenic opal and
643 chironomid-based summer temperatures, a moderate increase in Ti cps, and rather constant
644 values in clay and TOC contents. Biogenic opal as indicator of the lakes' diatom production and
645 chironomid-derived T_{July} show similarities to the diatom isotope record such as common Mid
646 Holocene maxima and Late Holocene minima. Meltwater events should lead to enhanced
647 nutrient supply to the lake and, thus, a higher biogenic opal concentration in the core. Some

minima, e. g. at 0.01, 1.7, 4.2, 6.0, 6.7 and 9.5 cal. ka BP in the $\delta^{18}O_{diatom}$ record roughly correspond to maxima in the biogenic opal concentration (Fig. 6). Some of these $\delta^{18}O_{diatom}$ minima are related to maxima (e. g. at 0.01, 6.0 cal. ka BP) in the total amount of lotic chironomids (Fig. 6).

Despite lower frequency variations of biogenic opal compared to $\delta^{18}O_{diatom}$ and the absence of a statistically significant relationship between both, the transport of nutrients by inflow processes (by meltwaters) to the lake seems to be reflected in $\delta^{18}O_{diatom}$. The only other biotic proxy displaying a few similar, although not well-expressed maxima (i. e. at ~8.0, 6.4 and 2.0 cal. ka BP) is the TOC record as proxy for organic matter deposition of Lake Bolshoye Shchuchye (Lenz et al., 2021).

A recent study by Cowling et al. (2021) deduced changes in the summer water balance and moisture sources during deglaciation and Early Holocene, using leaf wax hydrogen isotopes at Lake Bolshoye Shchuchye. However, a significant enrichment of $\delta^{2}H_{leaf\ wax}$ values between 10.5 and 10.0 cal. ka BP does not correspond to the changes in the $\delta^{18}O_{diatom}$ signal (Fig. 4). This inconsistency can be related to uncertainties in the age models and temporal resolution of the datasets. Moreover, leaf waxes are related to (soil) water uptake into terrestrial and aquatic plants and more complicated for deriving the lake water isotope composition.

If we attribute the $\delta^{18}O_{diatom}$ fluctuations to glacial advances, they should also be reflected in abiotic proxies such as clay content or Ti cps at Lake Bolshoye Shchuchye, which were interpreted as indicators for glacial meltwater input and catchment erosion, respectively (Lenz et al., 2021). Although there is a similarity between these abiotic parameters in the Holocene, they are neither reflecting a similar overall trend, nor similar short-term variations as found in the $\delta^{18}O_{diatom}$ record.

Consequently, the hydrological changes inferred from the diatom isotopes have no clear linkage to the abiotic changes in the lake sediments, or these lake-internal proxies are not sensitive enough to record them. Hence, neither changes in glacial meltwater fluxes nor erosion

levels in the catchment (as inferred from Ti cps and clay contents) can explain the short-term $\delta^{18}O_{diatom}$ variability. This suggests that glaciers in the catchment, if present in the Holocene, were either too small or too distant from the lake to have a major influence on the sediment record. Hence, the only water source that can plausibly explain the short-term fluctuations in the record are changes in the snow and its meltwater supply in the catchment, independent from glacier-derived meltwater.

5.6. Snow as key driver for short-term $\delta^{18}O_{diatom}$ fluctuations

Topographical features in the Polar Urals include leeward accumulation caused by persistent westerly winds, snow avalanches and shadowing-effects from mountain ridges. These factors can lead to a substantial (5–6 times, in the period 1958–1978) increase of the mean winter mass balance as compared to local precipitation (Mangerud et al., 2008). Presently, enhanced snow accumulation is strongly favored at higher elevations, on leeward slopes and in depressions (Voloshina, 1988). We draw the following conclusions from regional glacier mass balance studies: (1) the hydrology of the Polar Urals is strongly dominated by snow; (2) redistribution of snow may lead to a much higher SWE than actual precipitation (3) shadowing effects protect cirque glaciers and nival niches.

Figure 6 displays the geomorphological and snow characteristics of the Lake Bolshoye Shchuchye catchment. The DEM in Fig. 6A and the derived slopes angles in Fig. 6B reveal steeply (up to 65°) incised valleys and several small streams draining into the lake. Generally, the catchment extends to the northwest of the lake with a maximum and mean elevation of about 1200 and 500 m a.s.l., respectively.

For calculating the snow distribution of the Lake Bolshoye Shchuchye catchment we used the precipitation amount from snow profiles of the nearby Bol'shaya Khadata catchment (Gokhman & Zhidkov, 1979). Redistribution of snow may lead to a surplus of snow (reaching up to 8.45 m in snow height corresponding 3.40 m of snow-water equivalent; Figs 6 C and D) in

some areas of the catchment, especially in the higher altitudes and in narrow valleys in the northern/northwestern part of the catchment (Fig. 6). This suggests that in colder years, perennial snow fields may develop in leeside positions, storing the a surplus accumulated snow and allowing for increased snow melt contribution in warmer years.

These specific regional characteristics described above must necessarily have an impact on the lake hydrology, even though there are currently no glaciers in the Bolshoye Shchuchye catchment (Fig. 1B). As pointed out, a direct impact of glacier advances and retreat in the catchment in the Holocene is unlikely as abiotic indicators in the Holocene lake sediments do not suggest abrupt changes of sediment sources.

We therefore assume snow changes within the catchment to be the main driver of the catchment's hydrology and, thus, responsible for the short-term fluctuations in the $\delta^{18}O_{diatom}$ record. Due to shadowing effects, only part of this snow melts in summer and discharges into the lake. In phases of stronger winds and/or more precipitation, the Bolshoye Shchuchye catchment on the leeward side of the Polar Urals can receive excess snow amounts. While the exact mechanisms of how the snow and the snow melt affect the lake are yet to be identified, two dominating effects can be assumed: (1) more snow precipitation and redistribution directly lead to more snow in the catchment, and hence, possibly to a higher snow-derived and isotopically-depleted influx to the lake, (2) a local warming and/or reduced shadowing effect (Mangerud et al., 2008) may provide more snow melt to the lake, especially when the catchment is snow-saturated.

Enhanced snow influx hence directly impacts on the lake water isotopic composition when more melt waters from higher altitudes with lighter isotopic composition are drained to the lake. Conversely, centennial-scale maxima as observed in the Bolshoye Shchuchye diatom oxygen isotope record could be attributed to short-term interruptions of snow melt supply to the lake due to reduced influx from higher altitudes, and hence, lead to isotopically heavier $\delta^{18}O_{diatom}$ values. The quick rebounds towards isotopically lighter values may then reflect a return to the "normal"

conditions prevailing before these excursions: large amounts of snow being redistributed from the windward side of the Polar Urals towards the leeward side (into the Bolshoye Shchuchye catchment).

In summary, the complex interplay between local hydroclimatic conditions with more snow delivered to the catchment (more P, stronger winds) and temporarily enhanced snow-melt phases (higher summer T) likely drives the observed short-term changes in the Bolshoye Shchuchye catchment. This mechanism allows for using the Bolshoye Shchuchye diatom oxygen isotopes as local snow-melt indicator, hence as paleo precipitation and summer temperature proxy.

6. Conclusions

Lake Bolshoye Shchuchye is a well-mixed lake, covered by ice for more than half of the year, with negligible evaporative effects, as derived from the recent water isotope dataset. Diatom oxygen isotopes ($\delta^{18}O_{diatom}$) from the lacustrine sediments of Lake Bolshoye Shchuchye have been used as proxies for the hydrological and climate dynamics in the lake catchment.

During the Holocene, the Lake Bolshoye Shchuchye $\delta^{18}O_{diatom}$ record generally follows a decrease in summer insolation, in line with the northern hemisphere (NH) temperature history. However, Lake Bolshoye Shchuchye displays exceptional, short-term, centennial-scale changes of exceeding 5‰, especially in Mid and Late Holocene contemporaneous with and similar to NH glacier advances. As most of these minima and maxima are confirmed by more than one data point, these are considered as no methodological artefacts. Mixing calculations reveal that ~ 30–50% of the Lake Bolshoye Shchuchye water needs to be exchanged with isotopically different water within short time to account for these shifts in $\delta^{18}O_{diatom}$. However, larger Holocene glacier advances in the Lake Bolshoye Shchuchye catchment are not known and have left no significant imprint on the lakes' abiotic proxies. Accordingly, a source of light isotope composition is snow, known to be transported in significant quantities and with large variability to the leeward side of the Polar Urals. Hence, we consider snow transport to the catchment and switch on/off of

meltwater supply to the lake as dominant hydrological process responsible for the observed short-term changes in the $\delta^{18}O_{diatom}$ record. A linkage between meltwater influx to lakes and $\delta^{18}O_{diatom}$ has been found before (Meyer et al., 2015). Here, however, centennial-scale hydrological changes have been documented in this high-latitude diatom oxygen isotope record, which, for this specific setting, are interpreted as indicator for palaeo precipitation and summer temperature changes.

Acknowledgements

The study was performed in the frame of the German-Russian projects 'PLOT − Paleolimnological Transect' (BMBF; grant 03G0859) and its successor 'PLOT – Synthesis' (BMBF; grant 03F0830C) both funded by the German Federal Ministry of Education and Research. We thank Ilona Schaepan from the German Research Center for Geosciences (GFZ) in Potsdam for the EDX analyses, Rita Fröhlking-Teichert from the AWI Bremerhaven Marine Geology laboratory for BSi measurements, and Mikaela Weiner for technical support during sample preparation and isotope measurements at the AWI Potsdam stable isotope laboratory. Topographic and snow redistribution analyses were performed with support of the RUDN University Strategic Academic Leadership Program (Dr. Yuri Dvornikov).

References

Andreev, A.A., Tarasov, P.E., Ilyashuk, B.P., Ilyashuk, E.A., Cremer, H., Hermichen, W.-D., Wischer, F., Hubberten, H.-W. (2005). Holocene environmental history recorded in Lake Lyadhej-To sediments, Polar Urals, Russia. *Palaeogeography, Palaeoclimatology, Palaeoecology*, 223, 181–203.

Astakhov, V.I. (2018). Late Quaternary glaciation of the northern Urals: a review and new observations. *Boreas* 47, 379–389.

Berger, A., Loutre, M.F. (1991). Insolation values for the climate of the last 10 million years. *Quaternary Science Reviews* 10, 297–317.

Biskaborn, B. K., Nazarova, L., Pestryakova, L. A., Syrykh, L., Funck, K., Meyer, H., Chapligin, B., Vyse, S., Gorodnichev, R., Zakharov, E., Wang, R., Schwamborn, G., and

Diekmann, B. (2019). Spatial distribution of environmental indicators in surface sediments of Lake Bolshoe Toko, Yakutia, Russia, *Biogeosciences* 16(20), 4023-4049. https://doi.org/10.5194/bg-2019-146.

Blaauw, M. (2010). Methods and code for 'classical' age-modelling of radiocarbon sequences. *Quaternary Geochronology* 5: 512-518.

Blaauw, M. (2021). Clam: Classical Age-Depth Modelling of Cores from Deposits. R package version 2.3.9.

Bogdanov, V.D., Bogdanova, E.N., Gavrilov, A.L., Melnichenko, I.P., Stepanov, L.N., Yarushina, M.I. (2004). Biological resources of aquatic ecosystems of the Polar Urals. Publishing House of Ural Branch of RAS, Ekaterinburg. 168 pp. (in Russian).

Bonne, J.-L., Meyer, H., Behrens, M., Boike, J., Kipfstuhl, S., Rabe, B., Schmidt, T., Schönicke, L., Steen-Larsen, H. C., Werner, M., (2020). Moisture origin as a driver of temporal variabilities of the water vapour isotopic composition in the Lena River Delta, Siberia. *Atmospheric Chemistry and Physics*, *20*(17), 10493–10511. https://doi.org/10.5194/acp-20-10493-2020

Bowen, G.J. (2021). The Online Isotopes in Precipitation Calculator, version OIPC3.1 (4/2017) http://www.waterisotopes.org

Bowen, G.J., & Revenaugh, J. (2003). Interpolating the isotopic composition of modern meteoric precipitation. *Water Resources Research* 39 (10), 1299. doi:10.129/2003WR002086.

Bowen, G.J., Wassenaar, L.I., Hobson, K.A. (2005). Global application of stable hydrogen and oxygen isotopes to wildlife forensics. *Oecologia* 143, 337–348.

Brooks, S.J., Langdon, P.G., Heiri, O. (2007). The identification and use of palaearctic chironomidae larvae in palaeoecology. QRA Technical Guide No. 10. Quaternary Research Association, London. 276 pp.

Cartier, R., Sylvestre, F., Paillès, C., Sonzogni, C., Couapel, M., Alexandre, A., Mazur, J.-C., Brisset, E., Miramont, C., Guiter, F. (2019). Diatom-oxygen isotope record from high-altitude Lake Petit (2200 m a.s.l.) in the Mediterranean Alps: shedding light on a climatic pulse at 4.2 ka. *Climate of the Past* 15, 253–263.

Chapligin, B., Leng, M.J., Webb, E., Alexandre, A., Dodd, J.P., Ijiri, A., Lücke, A., Shemesh, A., Abelmann, A., Herzschuh, H., Longstaffe, F.J., Meyer, H., Moschen, R., Okazaki, Y., Rees, N.H., Sharp, Z.D., Sloane, H.J., Sonzongi, C., Swann, J.E.A., Sylvestre, F., Tyler, J.J., Yam, R. (2011). Inter-laboratory comparison of oxygen isotope compositions from biogenic silica. *Geochimica et Cosmochimica Acta* 75, 7242–7256.

Chapligin, B., Meyer, H., Bryan, A., Snyder, J., Kemnitz, H. (2012a). Assessment of purification and contamination correction methods for analysing the oxygen isotope composition from biogenic silica. *Chemical Geology* 300–301, 185–199.

Chapligin, B., Meyer, H., Friedrichsen, H., Marent, A., Sohns, E., Hubberten, H.-W. (2010). A high-performance, safer and semi-automated approach for the $\delta^{18}O$ analysis of diatom silica and new methods for removing exchangeable oxygen. *Rapid Communications in Mass Spectrometry* 24, 2655–2664.

Chapligin, B., Meyer, H., Swann, G.E.A., Meyer-Jacob, C., Hubberten, H.-W. (2012b). A 250-ka oxygen isotope record from diatoms at Lake El'gygytgyn, far east Russian Arctic. *Climate of the Past*, 8, 1621–1636. https://doi.org/10.5194/cp-8-1621-2012.

Clarke, C.L., Alsos, I.G., Edwards, M.E., Paus, A., Gielly, L., Haflidason, H., Mangerud, J., Regnéll, C., Hughes, P.D.M., Svendsen, J.I., Bjune, A.E. (2020). A 24,000-year ancient DNA and pollen record from the Polar Urals reveals temporal dynamics of arctic and boreal plant communities. *Quaternary Science Reviews*, 247**,** 106564.

Clayton, R., & Mayeda, T. (1963). The use of bromine pentafluoride in the extraction of oxygen from oxides and silicates for isotopic analysis. *Geochimica et Cosmochimica Acta*, 27, 43–52.

Cowling, O., Thomas, E., Svendsen, J.I., Mangerud, J., Haflidason, H., Regnéll, C., Brendryen, J. (2021). The hydrologic cycle in western Siberia during the past 24,000 years changed in step with plant community structure. *Journal of Quaternary Science*.

Craig, H. (1961). Isotopic variations in meteoric waters. *Science* 133, 1702–1703.

Cremer, H., Andreev, A., Hubberten, H.-W., Wischer, F. (2004). Paleolimnological reconstructions of Holocene environments and climate from Lake Lyadhej-To, Ural Mountains, Northern Russia. *Arctic, Antarctic, and Alpine Research*, 36, 147– 155.

Dahl, S.O., Bakke, J., Lie, Ø., Nesje, A. (2003). Reconstruction of former glacier equilibrium-line altitudes based on proglacial sites: an evaluation of approaches and selection of sites. *Quaternary Science Reviews*, 22, 275–287.

Dansgaard, W. (1964). Stable isotopes in precipitation. *Tellus*, 16 (4), 436–468.

Davis, P.T., Menounos, B., Osborn, G. (2009). Holocene and latest Pleistocene alpine glacier fluctuations: a global perspective. *Quaternary Science Reviews*, 28, 2021–2033.

Darling, W.G., Bath, A.H., Gibson, J.J., Rozanski, K. (2006). Isotopes in Water. In: Leng M.J. (Ed.). Isotopes in Paleoenvironmental Research. Vol. 10. Springer, Dordrecht, pp. 1-52.

Dodd, J.P., & Sharp, Z.D. (2010). A laser fluorination method for oxygen isotope analysis of biogenic silica and a new oxygen isotope calibration of modern diatoms in freshwater environments. *Geochimica et Cosmochimica Acta*, 74, 1381–1390.

Dortch, J.M., Owen, L.A., Caffee, M.W. (2013). Timing and climatic drivers for glaciation across semi-arid western Himalayan-Tibetan orogen. *Quaternary Science Reviews*, 78,188–208.

Dushin, V.A., Serdyukova, O.P., Malyugin, A.A., Nikulina, I.A., Kozmin, V.S., Burmako, P.L., Abaturova, I.V., Kozmina, L.I. (2009). State Geological Map of the Russian Federation 1:200000. Polar Ural Series. Sheet Q-42-I, II (Laborovaya). VSEGEI, St. Petersburg (in Russian).

Dvornikov, Y. A., Khomutov, A. V., Mullanurov, D. R., Ermokhina, K. A., Gubarkov, A. A., & Leibman, M. O. (2015). GIS and field data based modelling of snow water equivalent in shrub tundra. *Fennia*, *193*(1), 53–65. https://doi.org/10.11143/46363

Evans, J. S. (2020). *R spatialEco-package* (1.3-1). https://github.com/jeffreyevans/spatialEco

Friedman, I., Benson, C., Cleason, J. (1991). Isotopic changes during snow metamorphism. In H.P. Taylor, J.R. O'Neil, I.R. Kaplan (Eds.) Stable Isotope Geochemistry: A Tribute to Samuel Epstein (pp. 211–221). The Geochemical Society. Special Publication No. 3.

Gardner, A.S., Moholdt, G., Cogley, J.G., Wouters, B., Arendt, A.A., Wahr, J., Berthier, E., Hock, R., et al. (2013). A reconciled estimate of glacier contributions to sea level rise: 2003 to 2009. *Science*, 340, 852–857.

Gat, J.R. (1981). Lakes. In: Gat, J.R. and Gonfiantini, R. (Eds.). Stable Isotope Hydrology - Deuterium and Oxygen-18 in the water cycle. Tech. Rep. Series No. 210. IAEA, Vienna, pp. 203-221.

Gibson, J.J., Edwards, T.W.D. and Prowse, T.D (1999). Pan-derived isotopic composition of atmospheric water vapour and ist variability in northern Canada. *Journal of Hydrology*, 217, 55-74.

Gibson, C.E., Anderson, N.J., Haworth, E.Y. (2003). *Aulacoseira subarctica*: taxonomy, physiology, ecology and palaeoecology. *European Journal Phycology*, 38, 83–101.

Gokhman, V. V., & Zhidkov, V. A. (1979). On the spatial distribution of snow storage in Polar Urals. In V. M. Kotlyakov (Ed.), *Data of glaciological studies* (pp. 177–182). Academy of Sciences USSR.

Gonfiantini R. (1986). Environmental isotopes in Lake Studies. In: Fritz, O. and Fontes, J.C. (Eds.). Handbook of environmental isotope Geochemistry: Vol 2, The Terrestrial Environment, B. Elsevier, Amsterdam, pp. 113-168.

Gorelick, N., Hancher, M., Dixon, M., Ilyushchenko, S., Thau, D., & Moore, R. (2017). Google Earth Engine: Planetary-scale geospatial analysis for everyone. *Remote Sensing of Environment*, 202, 18–27. https://doi.org/10.1016/J.RSE.2017.06.031

Haflidason, H., Zweidorff, J.L., Baumer, M., Gyllencreutz, R., Svendsen, J.I., Gladysh, V., Logvina, E. (2019). The Lastglacial and Holocene seismostratigraphy and sediment distribution of Lake Bolshoye Shchuchye, Polar Ural Mountains, Arctic Russia. *Boreas,* 48, 452–469.

Heikkilä, M., Edwards, T.W.D., Seppä, H., Sonninen, E. (2010). Sediment isotope tracers from Lake Saarikko, Finland, and implications for Holocene hydroclimatology. *Quaternary Science Reviews,* 29, 17–18, 2146-2160. https://doi.org/10.1016/j.quascirev.2010.05.010.

Huggel, C., Haeberli, W., Kääb, A. (2008). Glacial hazards: perceiving and responding to threats in four world regions. In: Orlove, B., Wiegandt, E., Luckman, B.H. (Eds.). Darkening peaks. Glacier retreat, science and society. University of California Press, Berkeley, US. 68–80.

Hutchinson, M. F. (1989). A new procedure for gridding elevation and stream line data with automatic removal of spurious pits. *Journal of Hydrology*, 106, 211–232. https://doi.org/10.1016/0022-1694(89)90073-5

IAEA/WMO (2021). Global Network of Isotopes in Precipitation. The GNIP Database. https://nucleus.iaea.org/wiser

IPCC (2014). Climate Change 2014: Synthesis Report. Contribution of Working Groups I, II and III to the Fifth Assessment Report of the Intergovernmental Panel on Climate Change [Core Writing Team, R. K. Pachauri, & L. A. Meyer (Eds.)]. Latest Pleistocene and Holocene glacier variations in the European Alps. *Quaternary Science Reviews,* 28, 2137–2149.

Ivanov, M. N. (2013). *Evolution of glaciation of the Polar Urals in the late Holocene* (A. A. Lukashov & E. S. Troshkina (eds.)). Faculty of Geography, MSU.

Ivy-Ochs, S., Kerschner, H., Maisch, M., Christl, M., Kubik, P.W., Schluechter, C. (2009). Latest Pleistocene and Holocene glacier variations in the European Alps. *Quaternary Science Reviews,* 28, 2137–2149.

Jankovská, V., Andreev, A.A., Panova, N.K. (2006). Holocene environmental history on the eastern slope of the Polar Ural Mountains, Russia. *Boreas,* 35, 650–661.

Juillet-Leclerc, A., & Labeyrie, L. (1987). Temperature dependence of the oxygen isotopic fractionation between diatom silica and water. *Earth and Planetary Science Letters*, 84, 69–74.

Jones, V. J., Leng, M. J., Solovieva, N., Sloane, H. J. & Tarasov, P. (2004). Holocene climate of the Kola Peninsula; evidence from the oxygen isotope record of diatom silica. *Quaternary Science Reviews, 23,* 833–839.

Kemmerich, A.O. (1966). The Polar Urals. Publishing House Fizkultura i Sport, Moscow. 112 pp. (in Russian).

Koboltschnig, G.R., & Schöner, W. (2011). The relevance of glacier melt in the water cycle of the Alps: the example of Austria. *Hydrology and Earth System Sciences,* 15, 2039–2048.

Kononov, Y.M., Ananicheva, M.D., Willis, I.C. (2005). High-resolution reconstruction of Polar Ural glacier mass balance for the last millennium. *Annals of Glaciology,* 42, 163–170.

Kostrova, S.S., Biskaborn, B.K., Pestryakova, L.A., Fernandoy, F., Lenz, M.M., Meyer, H., (2021). Climate and environmental changes of the Lateglacial transition and Holocene in northeastern Siberia: Evidence from diatom oxygen isotopes and assemblage composition at Lake Emanda. *Quaternary Science Reviews,* 259, 106905. https://doi.org/10.1016/ j.quascirev.2021.106905

Kostrova, S.S., Meyer, H., Bailey, H.L., Ludikova, A.V., Gromig, R., Kuhn, G., Shibaev, Y.A., Kozachek, A.V., Ekaykin, A.A., Chapligin, B. (2019). Holocene hydrological variability of Lake Ladoga, northwest Russia, as inferred from diatom oxygen isotopes. *Boreas,* 48, 361–376.

Kostrova, S.S., Meyer, H., Chapligin, B., Kossler, A., Bezrukova, E.V., Tarasov, P.E. (2013). Holocene oxygen isotope record of diatoms from Lake Kotokel (southern Siberia, Russia) and its palaeoclimatic implications. *Quaternary International,* 290–291, 21–34.

Kostrova, S.S., Meyer, H., Chapligin, B., Tarasov, P.E., Bezrukova, E.V. (2014). The last glacial maximum and late glacial environmental and climate dynamics in the Baikal region inferred from an oxygen isotope record of lacustrine diatom silica. *Quaternary International,* 348, 25–36.

Khromova, T., Nosenko, G., Kutuzov, S., Muraviev, A., Chernova, L. (2014). Glacier area changes in Northern Eurasia. *Environmental Research Letters,* 9, 015003.

Khromova, T., Nosenko, G., Nikitin, S., Muraviev, A., Popova, V., Chernova, L., Kidyaeva, V. (2019). Changes in the mountain glaciers of continental Russia during the twentieth to twenty-first centuries. *Regional Environmental Change,* 19, 1229–1247.

Labeyrie, L.D. (1974). New approach to surface seawater palaeotemperatures using $^{18}O/^{16}O$ ratios in silica of diatom frustules. *Nature,* 248, 40–42.

Lammers, Y., Clarke, C.L., Erséus, C., Brown, A.G., Edwards, M.E., Gielly, L., Haflidason, H., Mangerud, J., Rota, E., Svendsen, J.I., Alsos, I.G. (2019). Clitellate worms (Annelida) in lateglacial and Holocene sedimentary DNA records from the Polar Urals and northern Norway. *Boreas,* 48, 317–329.

Lawrence, M. (2005). The Relationship between Relative Humidity and the Dewpoint Temperature in Moist Air: A Simple Conversion and Applications. *Bulletin of the American Meteorological Society,* 86, 225–233.

Leng, M.J., & Barker, P.A. (2006). A review of the oxygen isotope composition of lacustrine diatom silica for palaeoclimate reconstruction. *Earth-Science Reviews,* 75, 5–27.

Lenz, M. M., Andreev, A., Nazarova, L., Syrykh, L.S., Scheidt, S., Haflidason, H., Meyer, H., Brill, D., Wagner, B., Gromig, R., N., Lenz, M., Rolf, C., Kuhn, G., Fedorov, G., Svendsen, J.I., Melles, M. (2021). Climate and environmental history of the Polar Ural Mountains since early MIS 2 inferred from a 54-m-long sediment core from Lake Bolshoye Shchuchye. *Journal of Quaternary Science*. DOI: 10.1002/jqs.3400.

Lepskaya, E.V., Jewson, D.H., Usoltseva, M.V. (2010). *Aulacoseira subarctica* in Kurilskoye Lake, Kamchatka: A deep, oligotrophic lake and important pacific salmon nursery. *Diatom Research,* 25 (2), 323–335.

Linacre, E. T. (1977). A simple formula for estimating evaporation rates in various climates, using temperature data alone. *Agric. Meteorol.*, 18, 409–424.

Lubinsky, D.J., Forman, S.L., Miller, G.H. (1999). Holocene glacier and climate fluctuations on Franz Josef Land, Arctic Russia, 80° N. *Quaternary Science Reviews,* 18 (1), 85–108.

Mangerud, J., Gosse, J., Matiouchkov, A., Dolvik, T. (2008). Glaciers in the Polar Urals, Russia, were not much larger during the Last Global Glacial Maximum than today. *Quaternary Science Reviews,* 27, 1047–1057.

Matthews, J.A., Dresser, P.Q. (2008). Holocene glacier variation chronology of the Smørstabbtinden massif, Jotunheimen, southern Norway, and the recognition of century- to millennial-scale European Neoglacial events. *Holocene,* 18, 181–201.

Meyer, H., Chapligin, B., Hoff, U., Nazarova, L., Diekmann, B. (2015). Oxygen isotope composition of diatoms as Late Holocene climate proxy at Two-Yurts Lake, Central Kamchatka, Russia. *Global and Planetary Change,* 134, 118–128.

Meyer, H., Schönicke, L., Wand, U., Hubberten, H.-W., Friedrichsen, H. (2000). Isotope studies of hydrogen and oxygen in ground ice – experiences with the equilibration technique. *Isotopes in Environmental and Health Studies,* 36, 133–149.

Mitrofanova, E.Y. (2017). Phytoplankton of the Lake Bolshoe Shchuchye and rivers of its basin in August 2016. Scientific Newsletter of Yamalo-Nenets Autonomous Region 1 (94), 55−61 (in Russian).

Moller Pillot, H.K.M. (2009). Chironomidae Larvae. Biology and ecology of the Chironomini. KNNV Publishing, Zeist. 270 pp.

Moller Pillot H.K.M. (2013). Chironomidae larvae of the Netherlands and adjacent lowlands. Volume 3 Biology and ecology of the aquatic Orthocladiinae. 312 pp. KNNV Publishing, Zeist, Netherlands.

Morozova, L.M., Magomedova, M.A., Ektova, S.N., Dyachenko, A.P., Knyazev., M.S. (Eds.), 2006. Vegetation cover and plant resources of the Polar Urals. Publishing House of the Ural University, Yekaterinburg. 796 pp. (in Russian).

985 Mortlock, R.D., & Froelich, P.N. (1989). A simple method for the rapid determination of
986 biogenic opal in pelagic marine sediments. *Deep-Sea Research*, 36, 1415–1426.
987 Müller, P.J., & Schneider, R. (1993). An automated leaching method for the determination of
988 opal in sediments and particulate matter. *Deep Sea Research Part I,* 40, 425–444.
989 Nazarova, L., Bleibtreu, A., Hoff, U., Dirksen, V., Diekmann, B. (2017a). Changes in
990 temperature and water depth of a small mountain lake during the past 3000 years in Central
991 Kamchatka reflected by chironomid record. *Quaternary International,* 447, 46–58.
992 Nazarova, L., Herzschuh, U., Wetterich, S., Kumke, T., Pestjakova, L. (2011). Chironomid-
993 based inference models for estimating mean July air temperature and water depth from lakes in
994 Yakutia, northeastern Russia. *Journal of Paleolimnology,* 45, 57–71.
995 Nazarova, L., Self, A., Brooks, S.J., van Hardenbroek, M., Herzschuh, U., Diekmann, B.
996 (2015). Northern Russian chironomid-based modern summer temperature data set and inference
997 models. *Global Planetary Change,* 134, 10–25.
998 Nazarova, L.B., Self, A.E., Brooks, S.J., Solovieva, N., Syrykh, L.S., Dauvalter, V.A.
999 (2017b). Chironomid Fauna of the Lakes from the Pechora River Basin (East of European part of
1000 Russian Arctic): Ecology and Reconstruction of Recent Ecological Changes in the Region.
1001 *Contemporary Problems of Ecology,* 10, 350–362.
1002 Nazarova L., Grebennikova T.A., Razjigaeva N.G., Ganzey L.A., Belyanina N.I., Arslanov
1003 K.A., Kaistrenko V.M., Gorbunov A.O., Kharlamov A.A., Rudaya N., Palagushkina O.,
1004 Biskaborn B.K., Diekmann B. (2017c). Reconstruction of Holocene environmental changes in
1005 Southern Kurils (North-Western Pacific) based on palaeolake sediment proxies from Shikotan
1006 Island. *Global and Planetary Change,* 159: 25–36. DOI: 10.1016/j.gloplacha.2017.10.005
1007 Nazarova, L., Sachse D., Fuchs H.G.E., Dirksen V., Dirksen O., Syrykh L., Razjigaeva N.G.,
1008 Diekmann B. (2021a). Holocene evolution of a proglacial lake in southern Kamchatka, Russian
1009 Far East. *Boreas* doi: 10.1111/bor.12554
1010 Nazarova L., Frolova L.A., Palagushkina O.V., Rudaya N.A., Syrykh L.S., Grekov I.M.,
1011 Solovieva N., O.A. Loskutova O.A. (2021b). Recent shift in biological communities: A case
1012 study from the Eastern European Russian Arctic (Bol`shezemelskaya Tundra). *Polar biology.*
1013 doi: 10.1007/s00300-021-02876-7
1014 Nesje, A. (2009). Latest Pleistocene and Holocene alpine glacier fluctuations in Scandinavia.
1015 *Quaternary Science Reviews,* 28, 2119–2136.
1016 Nesje, A., Bakke, J., Brooks, S.J., Kaufman, D.S., Kihlberg, E., Trachsel, M., D'Andrea,
1017 W.J., Matthews, J.A. (2014). Late glacial and Holocene environmental changes inferred from
1018 sediments in Lake Myklevatnet, Nordfjord, western Norway. *Vegetation History and*
1019 *Archaeobotany,* 23, 229–248.

Nikolaev, V.I., & Mikhalev, D.V. (1995). An oxygen-isotope paleothermometer from ice in Siberian permafrost. *Quaternary Research,* 43, 14–21.

NOAA NCEI, (2021). NOAA National Centers for Environmental Information. State of the climate: Global climate report for April 2020, published online May 2020, retrieved on May 26, 2020. https://www.ncdc.noaa.gov/sotc/global/202004

Nosenko, G., & Tsvetkov, D. (2003). Assessment of glaciers change on Polar Urals from ASTER imagery. In: Glaciological data. Report GD-32. National Snow and Ice Data Center, Boulder. 80–82.

Panova, N.K., Jankovska, V., Korona, O.M., Zinov'ev, E.V. (2003). The Holocene dynamics of vegetation and ecological conditions of the Polar Urals. *Russian Journal of Ecology*, 34, 219–230.

Pechkin, A.S., Kirillov, V.V., Koveshnikov, M.I., Krasnenko, A.S., Saltykov, A.V., Timkin, A.V., Dyachenko, A.V., (2017). Morphometric characteristics of the Lake Bolshoe Shchuchye. Scientific Newsletter of Yamalo-Nenets Autonomous Region 3 (96), 48−52 (in Russian).

Petrakov, D.A., Chernomorets, S.S., Evans, S.G., Tutubalina, O.V. (2008). Catastrophic glacial multi-phase mass movements: a special type of glacial hazard. *Advances in Geosciences,* 14, 211–218.

Pischalnikova, E.V. (2016). Circulation conditions of abundant snowfalls formation in Perm region. *Geographical bulletin*, 1 (36). 70–77 (in Russian).

Porter, C., Morin, P., Howat, I., Noh, M.-J., Bates, B., Peterman, K., Keesey, S., Schlenk, M., Gardiner, J., Tomko, K., et al. (2018). *ArcticDEM*. Harvard Dataverse, V1. https://doi.org/10.7910/DVN/OHHUKH

Quinn, P., Beven, K. J., & Lamb, R. (1995). The In (a/tan/beta) index: How to calculate it and how to use it within the Topmodel framework. *Hydrological Processes*, *9*(2), 161–182.

R Core Team. (2017). R: A language and environment for statistical computing. R Foundation for Statistical Computing. https://www.r-project.org/

R Core Team. (2020). R: A language and environment for statistical computing. R Foundation for Statistical Computing. https://www.r-project.org/

Radić, V., & Hock, R. (2014). Glaciers in the Earth's hydrological cycle: Assessments of glacier mass and runoff changes on global and regional scales. Surveys in Geophysics 35. 813–837.

Regnéll, C., Haflidason, H., Mangerud, J., Svendsen, J.I. (2019). Glacial and climate history of the last 24 000 years in the Polar Ural Mountains, Arctic Russia, inferred from partly varved lake sediments. *Boreas,* 48, 432–443.

Robert, J. H., & van Etten, J. (2012). *R-package raster: Geographic analysis and modeling with raster data* (2.0-12). http://cran.r-project.org/package=raster

Rozanski, K., Araguás-Araguás, L., Gonfiantini, R. (1993). Isotopic patterns in modern global precipitation. Geophysical Monograph 78. In Climate Change in Continental Isotope Records (pp. 1–36). American Geophysical Union Monograph.

Shahgedanova, M., Nosenko, G., Bushueva, I., Ivanov, M. (2012). Changes in area and geodetic mass balance of small glaciers, Polar Urals, Russia, 1950–2008. *Journal of Glaciology*, 58 (211), 953–964.

Shemesh, A., Rosqvist, G., Rietti-Shati, M., Rubensdotter, L., Bigler, C., Yam, R., Karlen, W. (2001). Holocene climatic change in Swedish Lapland inferred from an oxygen-isotope record of lacustrine biogenic silica. *Holocene, 11 (4)*, 447–454.

Solomina, O., Ivanov, M., Bradwell, T. (2010). Lichenometric studies on moraines in the Polar Urals. *Geografiska Annaler: Series A, Physical Geography*, 92 (1), 81–99.

Solomina, O.N., Bradley, R.S., Hodgson, D.A., Ivy-Ochs, S., Jomelli, V., Mackintosh, A.N., Nesje, A, Owen, L.A., Wanner, H., Wiles, G.C., Young, N.E. (2015). Holocene glacier fluctuations. *Quaternary Science Reviews,* 111, 9–34.

Solovieva N, Jones VJ., Birks HJB., Appleby PG., Nazarova L. (2008). Diatom responses to 20th century climate warming in lakes from the northern Urals, Russia. *Palaeogeography, Palaeoclimatology, Palaeoecology*, 259: 96 –106.

Stief, P., Nazarova L., & De Beer D. (2005). Chimney construction by Chironomus riparius larvae in response to hypoxia: microbial implications for freshwater sediments. *Journal of North American Benthological Society*, 24 (4): 858-871.

Svendsen, J. I., Alexanderson, H., Astakhov, V. I., Demidov, I., Dowdeswell, J. A., Funder, S., Gataullin, V., Henriksen, et al. (2004). Late Quaternary ice sheet history of northern Eurasia. *Quaternary Science Reviews,* 23 (11), pp. 1229-1272. doi: 10.1016/j.quascirev.2003.12.008

Svendsen, J.I., Krüger, L.C., Mangerud, J., Astakhov, V.I., Paus, A., Nazarov, D., Murray, A. (2014). Glacial and vegetation history of the Polar Ural Mountains in northern Russia during the Last Ice Age, Marine Isotope Stages 5–2. *Quaternary Science Reviews,* 92, 409–428.

Svendsen, J.I., Færseth, L.M.B., Gyllencreutz, R., Haflidason, H., Henriksen, M., Hovland, M.N., Lohne, Ø.S., Mangerud, J., et al. (2019). Glacial and environmental changes over the last 60 000 years in the Polar Ural Mountains, Arctic Russia, inferred from a high-resolution lake record and other observations from adjacent areas. *Boreas,* 48, 407–431.

Svensson, A., Andersen, K.K., Bigler, M., Clausen, H.B., Dahl-Jensen, D., Davies, S.M., Johnsen, S.J., Muscheler, R., et al., (2008). A 60.000 year Greenland stratigraphic ice core chronology. *Climate of the Past,* 4, 47–57.

Swann, G.E.A., Leng, M.J. (2009). A review of diatom $\delta^{18}O$ in palaeoceanography. *Quaternary Science Reviews*, 28, 384–398.

Swann, G.E.A., Leng, M.J., Juschus, O., Melles, M., Brigham-Grette, J., Sloane, H.J. (2010). A combined oxygen and silicon diatom isotope record of Late Quaternary change in Lake El'gygytgyn, North East Siberia. *Quaternary Science Reviews*, 29, 774-786. https://doi.org/10.1016/j.quascirev.2009.11.024.

van Hardenbroek, M., Chakraborty, A., Davies, K.L., Harding, P., Heiri, O., Henderson, A.C.G., Holmes, J.A., Lasher, G.E., et al., (2018). The stable isotope composition of organic and inorganic fossils in lake sediment records: Current understanding, challenges, and future directions. *Quaternary Science Reviews*, 196, 154–176.

Vinokurova, G.V. (2017). Phytoepilithon of the Lake Bolshoe Shchuchye and rivers flowing into and out of it (the Polar Urals). Scientific Newsletter of Yamalo-Nenets Autonomous Region 1 (94), 11−14 (in Russian).

Voloshina, A. (1988). Some results of glacier mass balance research on the glaciers in the Polar Urals. *Polar Geography and Geology*, 12, 200–211.

Wiederholm, T. (1983). Chironomidae of the Holarctic Region, Keys and Diagnoses. Part 1. Larvae: Entomologica Scandinavica, Supplement 19, 1–457.

WGMS, (2017). Global Glacier Change Bulletin No. 2 (2014–2015). Zemp, M., Nussbaumer, S.U., Gärtner-Roer, I., Huber, J., Machguth, H., Paul, F., Hoelzle, M. (Eds.). ICSU(WDS)/IUGG(IACS)/UNEP/UNESCO/WMO, World Glacier Monitoring Service, Zurich, Switzerland. 244 pp.

Yermolaeva, N.I., & Burmistrova, O.S. (2017). Zooplankton of the Lake Bolshoe Shchuchye. Scientific Newsletter of Yamalo-Nenets Autonomous Region 1 (94), 15−20 (in Russian).

1114 Table 1. Main geochemical characteristics of diatoms from Lake Bolshoye Shchuchye based on EDS data. Measured $\delta^{18}O$ values ($\delta^{18}O_{meas}$), calculated

1115 contamination (c_{cont}; %) and $\delta^{18}O$ values corrected for contamination ($\delta^{18}O_{corr}$) are given.

Core	Sample depth (cm)	Age (cal. ka BP)	SiO_2 (%)	Al_2O_3 (%)	Na_2O (%)	MgO (%)	K_2O (%)	CaO (%)	MnO (%)	FeO (%)	Total	$\delta^{18}O_{meas}$ (‰)	c_{cont} (%)	$\delta^{18}O_{corr}$ (‰)
Co1321-3-SL	surface		98.77	0.52	0.23	0.14	0.03	0.02	0.02	0.26	100.00	23.17	2.4	23.44
Co 1321-2	4.4	0.008	98.57	0.48	0.55	0.12	0.01	0.05	0.05	0.17	100.00	23.41	2.2	23.66
Co 1321-2	20.9	0.327	98.02	0.71	0.63	0.20	0.01	0.05	0.03	0.36	100.00	24.73	3.3	25.15
Co 1321-2	35.8	0.614	98.76	0.51	0.37	0.11	0.00	0.02	0.03	0.22	100.00	25.06	2.4	25.36
Co 1321-2	54.1	0.956	97.44	0.86	1.04	0.15	0.03	0.05	0.06	0.39	99.99	26.15	4.0	26.71
Co 1321-2	67.8	1,181	97.98	0.88	0.46	0.16	0.01	0.07	0.01	0.43	100.00	24.51	4.1	25.02
Co 1321-31-II	97.9	1.676	96.65	1.49	0.86	0.21	0.09	0.08	0.02	0.61	100.00	23.61	7.2	24.48
Co 1321-31-II	112.4	1.868	97.85	0.78	0.69	0.16	0.02	0.04	0.06	0.40	100.00	29.22	3.6	29.85
Co 1321-32-I	152.7	2.378	98.21	0.53	0.79	0.14	0.00	0.02	0.05	0.27	100.00	24.89	2.5	25.20
Co 1321-32-I	167.7	2.562	98.14	0.85	0.38	0.17	0.01	0.06	0.02	0.39	100.00	28.06	3.9	28.70
Co 1321-32-I	187.5	2.804	98.01	0.75	0.66	0.15	0.02	0.03	0.04	0.35	100.01	27.71	3.5	28.26
Co 1321-32-I	200.6	2.965	95.14	1.47	2.58	0.10	0.14	0.13	0.03	0.41	100.00	24.47	6.8	25.35
Co 1321-32-I	215.4	3.178	97.89	0.81	0.60	0.18	0.01	0.09	0.04	0.38	100.00	25.16	3.8	25.65
Co 1321-32-II	235.2	3.462	97.58	1.09	0.65	0.13	0.07	0.05	0.09	0.35	100.00	26.43	5.1	27.17
Co 1321-32-II	249.8	3.672	98.04	0.74	0.75	0.10	0.01	0.05	0.08	0.25	100.00	27.37	3.4	27.89
Co 1321-32-II	265.8	3.904	98.09	0.85	0.49	0.16	0.01	0.05	0.02	0.34	100.00	25.29	3.9	25.81
Co 1321-32-II	281.8	4.136	97.50	0.97	0.81	0.15	0.04	0.07	0.04	0.43	100.00	25.05	4.5	25.64
Co 1321-32-II	298.1	4.372	97.73	0.65	1.19	0.03	0.03	0.13	0.05	0.20	100.00	25.84	3.0	26.25
Co 1321-32-II	314.5	4.611	96.01	1.89	0.93	0.30	0.18	0.06	0.01	0.63	100.01	26.84	8.8	28.22
Co 1321-32-II	330.3	4.842	97.89	0.89	0.66	0.09	0.02	0.03	0.02	0.40	99.99	26.83	4.1	27.45
Co 1321-33-I	353.6	5.181	97.76	0.96	0.74	0.11	0.02	0.04	0.03	0.34	99.99	26.31	4.5	26.96
Co 1321-33-I	368.6	5.392	96.58	1.53	0.92	0.21	0.09	0.09	0.02	0.56	100.00	26.15	7.1	27.19
Co 1321-33-I	400.9	5.847	98.18	0.82	0.45	0.12	0.04	0.11	0.04	0.24	100.00	25.62	3.8	26.14
Co 1321-33-I	425.6	6.227	96.45	1.87	0.50	0.34	0.14	0.08	0.03	0.59	100.00	27.51	8.7	28.94
Co 1321-33-II	434.8	6.369	96.83	1.26	1.15	0.17	0.06	0.06	0.04	0.45	100.00	30.70	5.9	31.83
Co 1321-33-II	450.8	6.613	97.16	1.25	0.85	0.14	0.02	0.08	0.04	0.47	100.00	25.87	5.8	26.69
Co 1321-33-II	465.9	6.821	97.98	1.00	0.28	0.14	0.06	0.07	0.03	0.43	100.00	26.09	4.6	26.75
Co 1321-33-II	483.1	7.057	98.12	0.89	0.26	0.15	0.05	0.07	0.04	0.40	100.00	28.61	4.2	29.31
Co 1321-33-II	499.1	7.277	96.04	1.69	1.46	0.08	0.15	0.11	0.02	0.46	100.00	25.53	7.9	26.64
Co 1321-33-II	534.5	7.628	97.09	1.35	0.94	0.13	0.04	0.05	0.01	0.39	100.00	25.71	6.3	26.60
Co 1321-34-I	555.1	7.832	97.78	0.95	0.49	0.14	0.01	0.08	0.04	0.51	100.00	27.44	4.4	28.13
Co 1321-34-I	572.6	8.008	97.76	0.82	0.72	0.06	0.01	0.07	0.02	0.55	100.00	26.61	3.8	27.17
Co 1321-34-I	585.3	8.137	97.63	1.01	0.77	0.13	0.02	0.07	0.03	0.36	100.00	28.14	4.7	28.91
Co 1321-34-I	602.8	8.316	97.31	0.99	1.10	0.03	0.03	0.08	0.04	0.42	100.00	25.24	4.6	25.85

Co 1321-34-I	617.6	8.477	97.16	1.12	0.81	0.15	0.09	0.18	0.05	0.45	100.00	25.74	5.2	26.46
Co 1321-34-II	667.6	9.012	97.96	1.09	0.37	0.14	0.03	0.14	0.01	0.26	100.00	25.77	5.1	26.48
Co 1321-34-II	684.7	9.191	96.05	1.93	1.01	0.30	0.12	0.08	0.07	0.41	99.95	26.58	9.0	27.97
Co 1321-34-II	698.6	9.336	97.49	1.32	0.36	0.17	0.11	0.10	0.04	0.42	100.00	26.95	6.1	27.90
Co 1321-34-II	713.1	9.483	96.50	0.92	2.15	0.07	0.02	0.12	0.00	0.23	100.00	26.36	4.3	26.98
Co 1321-35-I	768.9	10.050	97.26	1.62	0.29	0.21	0.14	0.14	0.03	0.32	100.00	26.24	7.5	27.36
Co 1321-35-I	778.4	10.146	98.24	1.05	0.13	0.12	0.03	0.14	0.00	0.30	100.00	25.92	4.9	26.61
Co 1321-35-I	787.4	10.237	96.13	1.97	0.62	0.35	0.14	0.15	0.05	0.59	100.00	25.49	9.2	26.81
Co 1321-35-I	802.3	10.389	95.51	1.74	2.08	0.09	0.18	0.08	0.04	0.29	100.00	25.16	8.1	26.28
Co 1321-35-I	817.0	10.538	96.46	1.83	0.50	0.29	0.17	0.20	0.02	0.53	100.00	26.78	8.5	28.12
Co 1321-35-I	835.3	10.724	96.68	1.77	0.74	0.22	0.07	0.07	0.03	0.42	100.00	26.49	8.3	27.75
Co 1321-35-II	851.3	10.887	96.01	2.00	0.65	0.37	0.16	0.18	0.05	0.56	100.00	25.30	9.3	26.62
Co 1321-35-II	872.4	11.110	96.21	2.02	0.55	0.27	0.17	0.23	0.06	0.50	100.00	25.86	9.4	27.25
Co 1321-35-II	915.2	11.555	94.76	1.99	2.20	0.21	0.12	0.17	0.07	0.48	100.00	26.43	9.3	27.86

1116

Figure 1. A. Schematic maps of the Polar Urals including the study site and other points of interest modified from Andreev et al. (2005). B. Location of Lake Bolshoye Shchuchye (67°53'N; 66°19' E; 186 m a.s.l.) with the position of the Co 1321 sediment core (black diamond) and the water sampling site (grey circle); as well as location of the snow cover column (black circle). The sketch was adapted from Regnéll et al. (2019). The Shchuchy and Tronov glaciers are outside the Lake Bolshoye Shchuchye catchment.

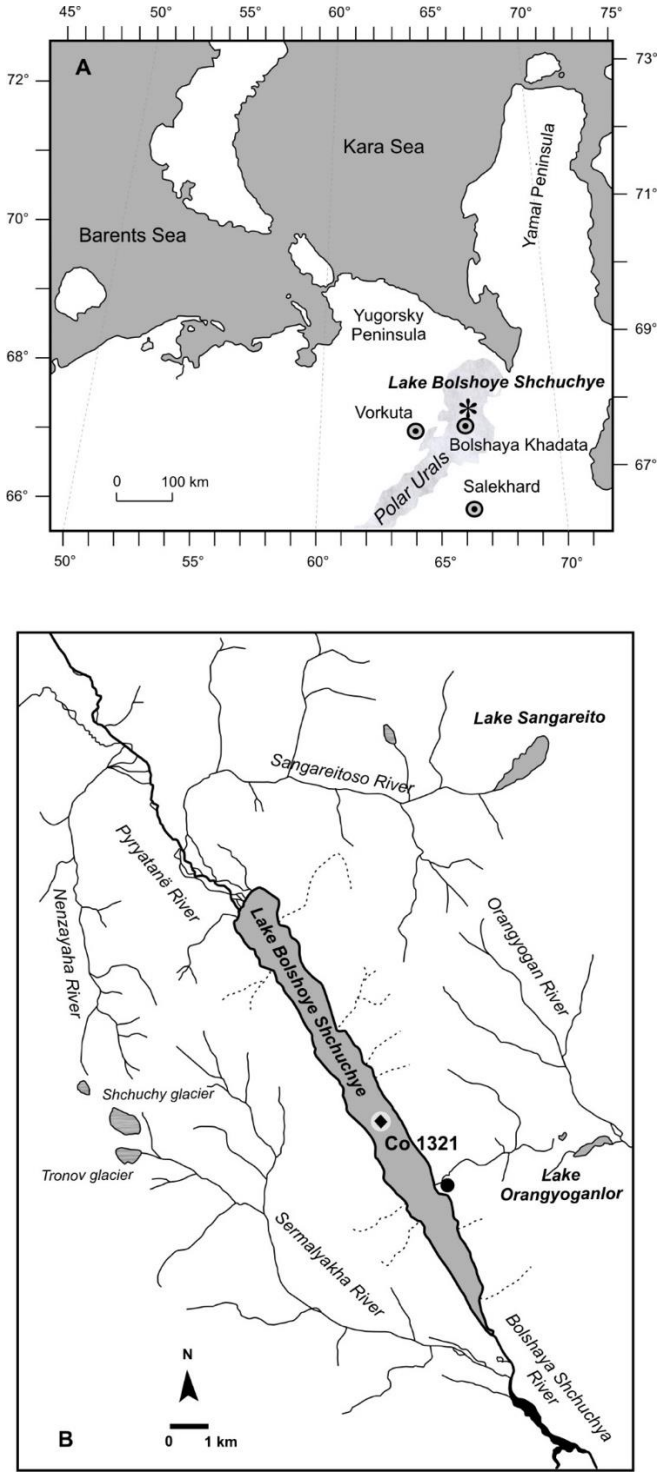

Figure 2. $\delta^{18}O$–δD diagram for water samples from Lake Bolshoye Shchuchye and snow cover. Additionally, GNIP data for regional precipitation, the Global Meteoric Water Line (GMWL; $\delta D = 8 \cdot \delta^{18}O + 10$; Craig 1961; Rozanski et al., 1993) and Local Meteoric Water Line (LMWL) based on GNIP data (black dash line; IAEA/WMO, 2021) and LMWL modelled from OIPC (grey solid line; Bowen, 2021) are given.

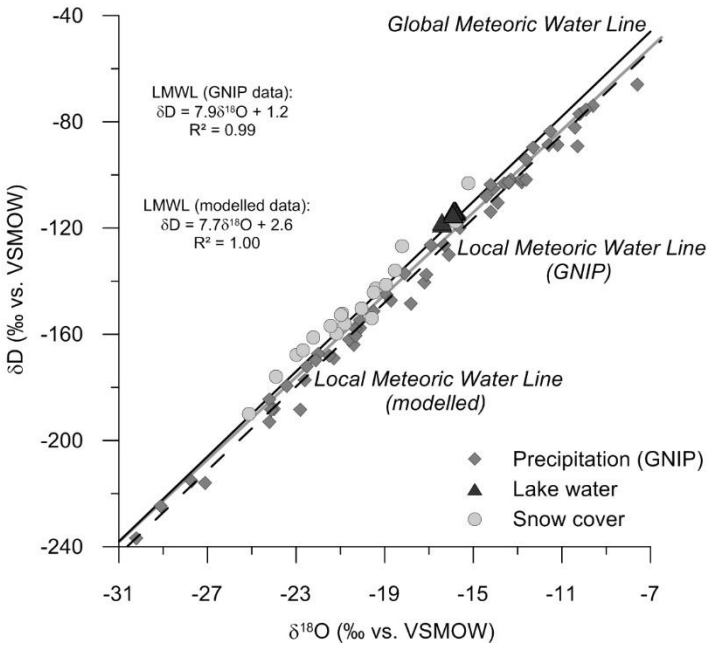

Figure 3. Depth profiles. A. Oxygen isotope composition of water from Lake Bolshoye Shchuchye. B. Lake water temperature, measured 50 m north of the coring site. C. Oxygen isotope composition of snow cover. Water and snow samples excluded from interpretation are marked as crossed out signs.

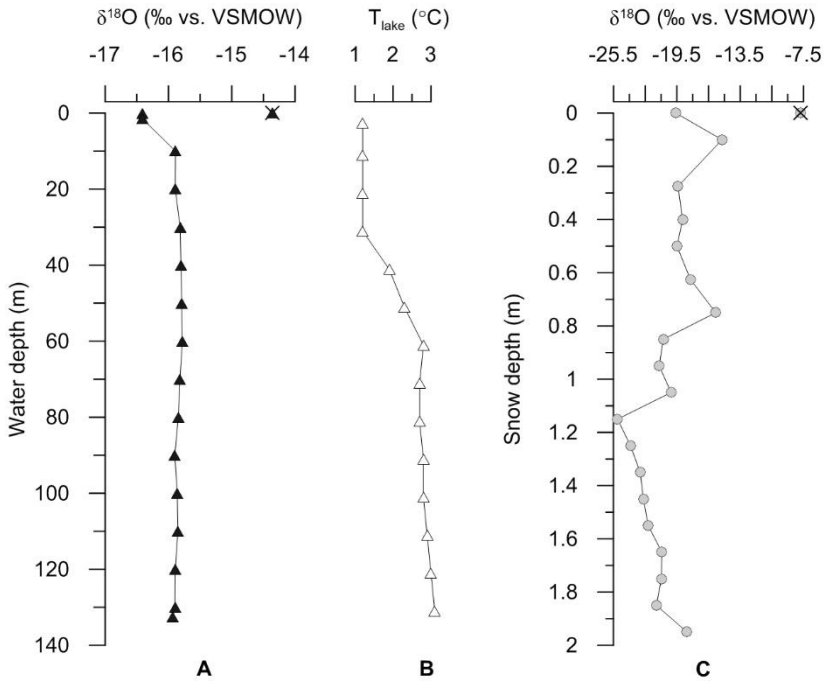

Figure 4. (A) Holocene oxygen isotope composition of diatoms from Lake Bolshoye Shchuchye (grey raw data: $\delta^{18}O_{meas}$; black: contamination-corrected $\delta^{18}O_{corr}$ values, referred to as $\delta^{18}O_{diatom}$) compared to other lake internal parameters, such as: (B) the biogenic silica percentage, as proxy for the diatom production, (C) clay content, as glacial meltwater proxy, (D) Ti cps (counts per second), a proxy for detrital input and catchment erosion. (E) TOC content, as proxy for organic matter input to the lake, as well as (F) the sum of lotic chironomids, indicative for riverine influx, and (G) a chironomid-based July air temperature reconstruction for Lake Bolshoye Shchuchye. The dashed line corresponds to the modern mean July air temperature (of 10.6°C). All lake internal proxies are introduced and discussed in detail in Lenz et al. (2021). Greyscales indicate periods of known glacier advances in Scandinavia (Nesje, 2009).

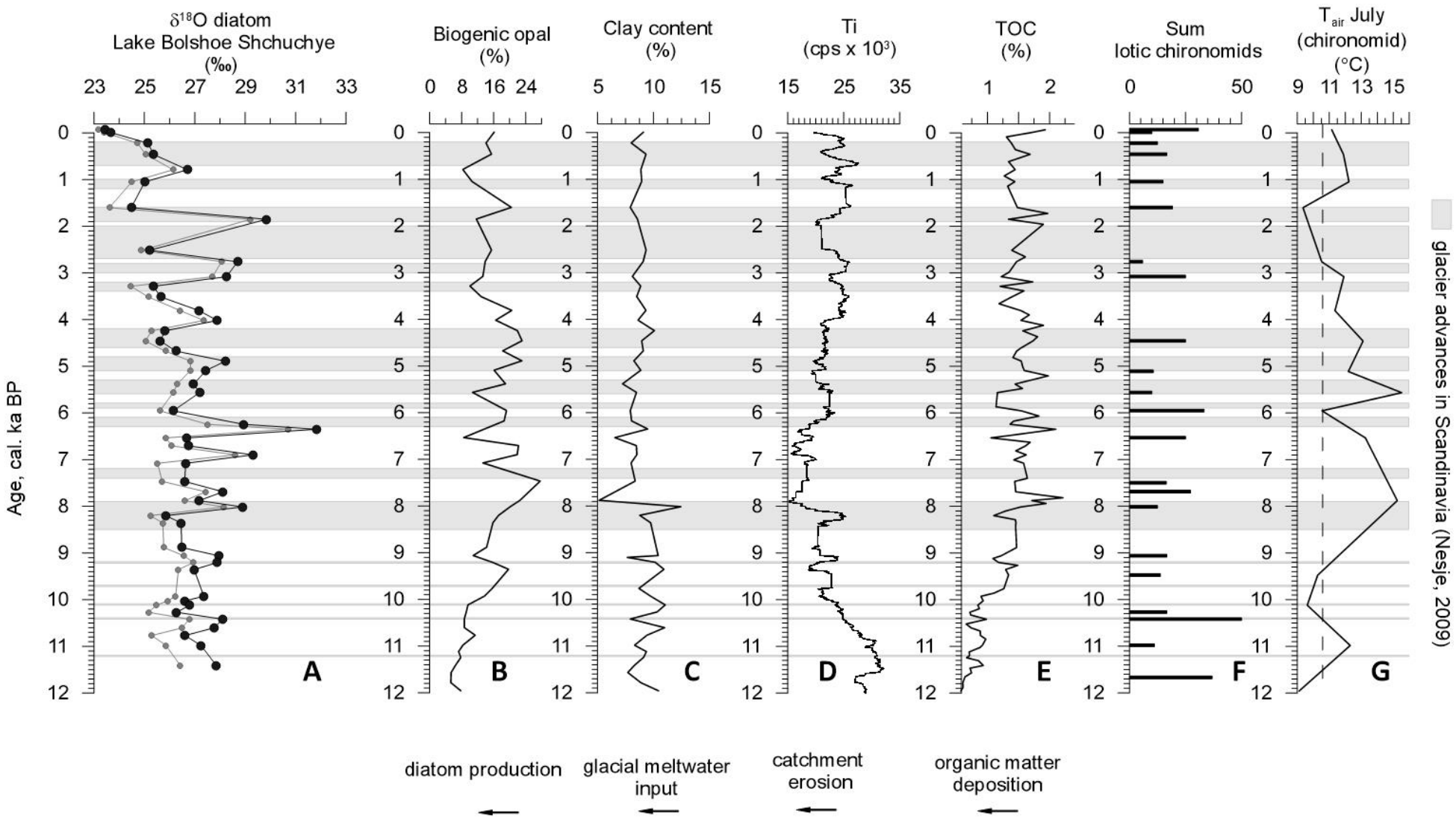
δ18O diatom
Lake Bolshoe Shchuchye
(‰)
Biogenic opal
(%)
Clay content
(%)
Ti
(cps x 10³)
TOC
(%)
Sum
lotic chironomids
T air July
(chironomid)
(°C)
Age, cal. ka BP
A
B
C
D
E
F
G
glacier advances in Scandinavia (Nesje, 2009)
diatom production
glacial meltwater input
catchment erosion
organic matter deposition

Figure 5. Modelled evaporative enrichment of lake water over time for three different scenarios of precipitation and atmospheric humidity. The black line represents present-day precipitation (P) and humidity (h) level, whereas the blue and red lines characterize hypothetical conditions with much lower precipitation and humidity.

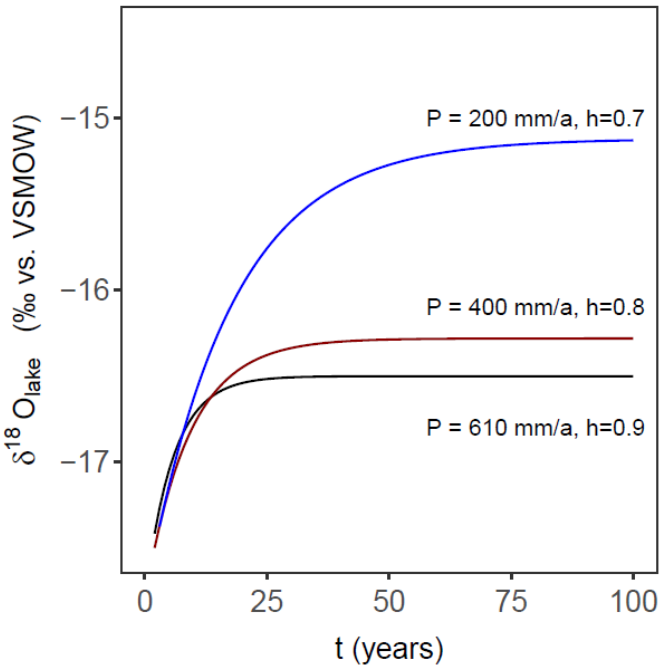

Figure 6. Geomorphological and snow characteristics of the Lake Bolshoye Shchuchye catchment. (A) Digital Elevation Model (DEM), (B) Slope (in degrees), (C) snow depth (in cm) and (D) Snow water equivalent (SWE, in mm) .

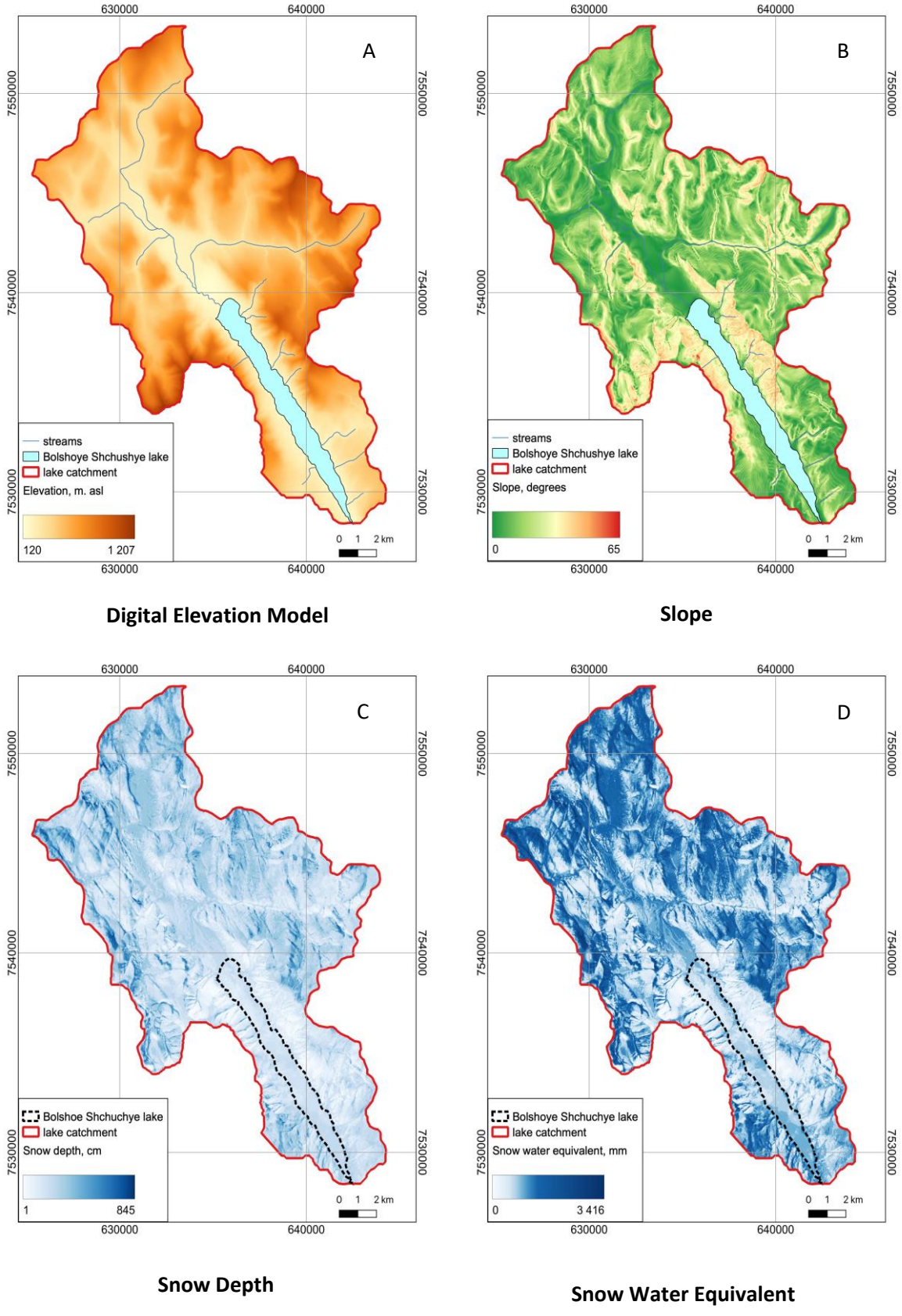

Figure 7. (A) Oxygen isotope composition of diatoms from Lake Bolshoye Shchuchye compared to other North Hemispheric (NH) climate reconstructions, such as (B) the NGRIP oxygen isotope record from Greenland ice (Svensson et al., 2008), an proxy for the NH air temperature, (C and D) the NH summer and winter insolation at 60° N (Berger & Loutre, 1991), as well as other regional diatom-based oxygen isotope records (E) from Lake Ladoga (Kostrova et al., 2019) and (F) Lake 850, Swedish Lapland (Shemesh et al., 2001), and (G) a cellulose-based reconstruction from Lake Saariko, Finland (Heikkilä et al., 2010).

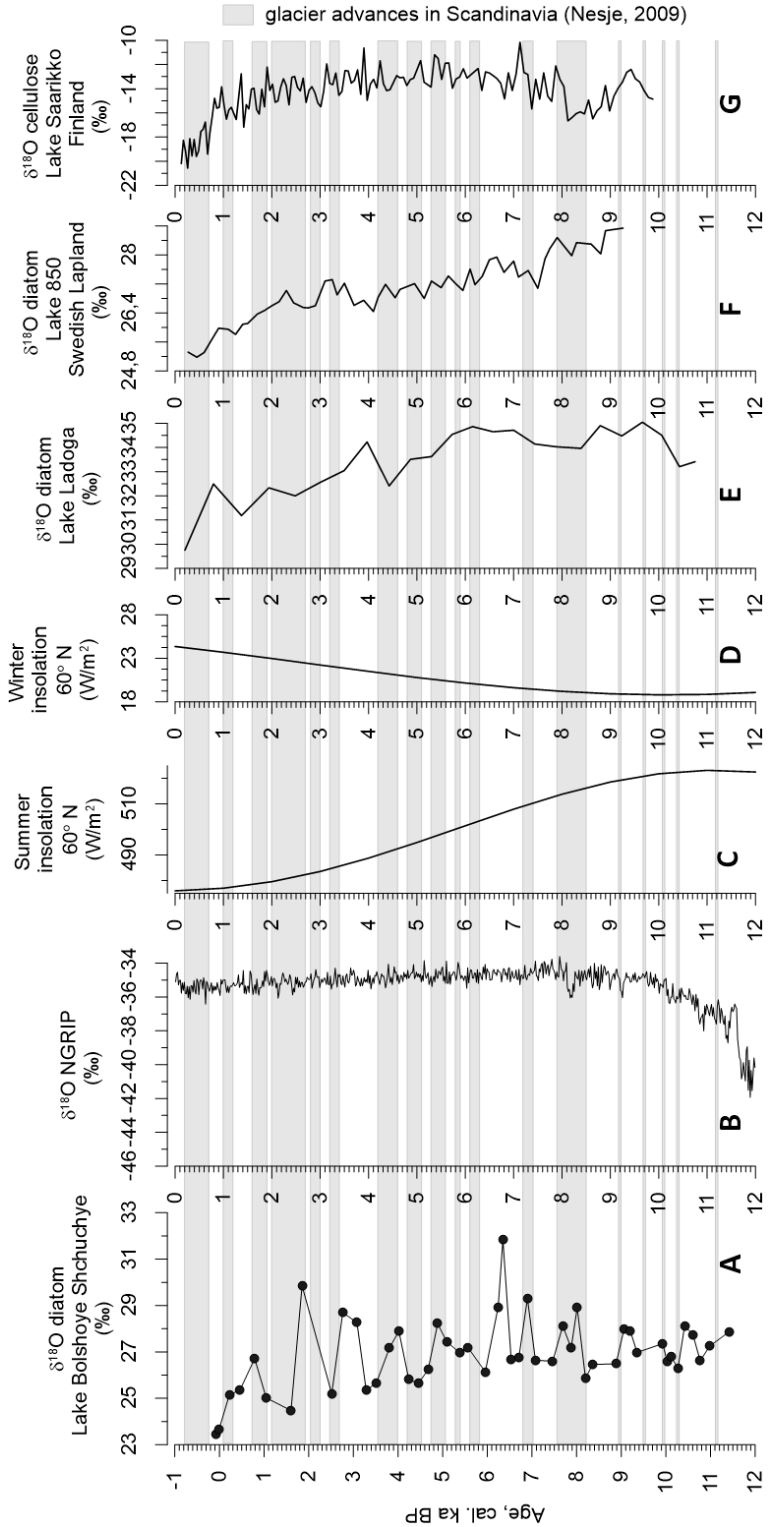

Figure S1. Scenario functions of T_{air} and T_{lake} changes corresponding to a 5‰-shift in $\delta^{18}O_{diatom}$, based on a diatom-temperature coefficient of −0.2‰/°C (Swann & Leng, 2009; Dodd & Sharp, 2010) and the regional temperature relation between monthly mean $\delta^{18}O_{prec}$ and T_{air} of $\delta^{18}O_{prec}$ = +0.34‰/°C (Salekhard; IAEA/WMO, 2021).